

A. Su-Schrieffer-Heeger Model within OBCs

In this section we discuss the SSH model with open boundary conditions (OBCs) also considering some relevant extensions, namely the introduction of next nearest neighbors (N.N.N. from here on) hoppings and the effect of disorder on both nearest and next nearest hoppings. A sketch of the resulting model is reported in Fig. 1, where v and w are the nearest neighbors (N.N.) hopping strengths, while v' and w' the N.N.N. ones. The on-site energies are fixed to zero and the lattice parameter a is shown in figure.

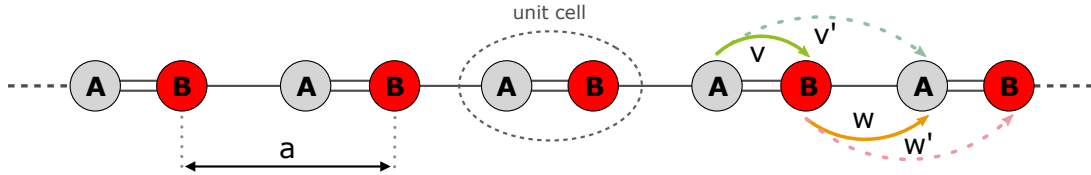


Figure 1: Schematic representation of our extended SSH model.

Nearest Neighbors Hamiltonian

The N.N. Hamiltonian with PBCs can be easily written as a two-level systems in k -space, as

$$\mathbf{H}(k) = \mathbf{d}(k) \cdot \boldsymbol{\sigma}, \quad \boldsymbol{\sigma} = (\sigma_x, \sigma_y, \sigma_z) \quad \Rightarrow \quad \varepsilon_{\pm}(k) = \pm |\mathbf{d}(k)|$$

where $\varepsilon_{\pm}(k)$ are the dispersion relations of the two bands and

$$\mathbf{d}(k) = (v + w \cos(ka), -w \sin(ka), 0)$$

draws a closed circle as k spans the Brillouin Zone.

In Fig. 2 the three qualitatively different cases are shown: for $v > w$ we have zero winding number around the origin, signature of a trivial topological character; for $v = w$ we have an undefined winding number, corresponding to the presence of a closed gap for some k point; finally, for $v < w$ we have a nonzero winding number, which corresponds to the interesting topological phase of the model. Thus, the open boundary analysis we show in the following will refer to these three situations.

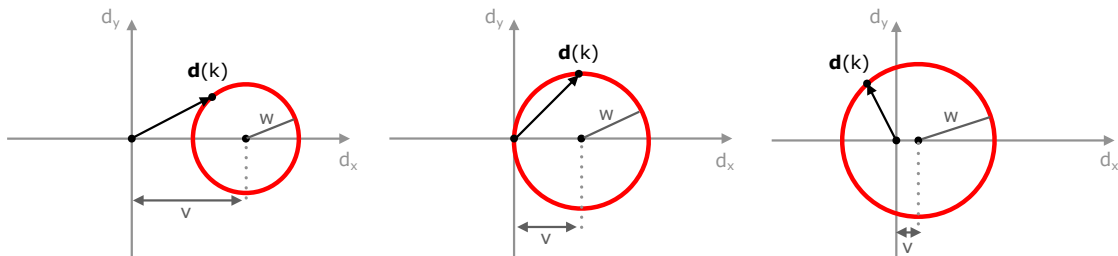


Figure 2: Path of the adiabatic parameter $\mathbf{d}(k)$ as k spans the 1st Brillouin Zone. We distinguish three relevant cases: on the left we have $v > w$, with zero winding number of the path with respect to the origin; on the right we have $v < w$, with winding number equal to one; in between we have $v = w$, for which the winding number is not a well defined quantity, corresponding to the breaking of the adiabatic regime (closure of the gap).

The corresponding real-space N.N. Hamiltonian is

$$H = \sum_j \left(v c_{A,j}^\dagger c_{B,j} + w c_{B,j}^\dagger c_{A,j+1} + \text{h.c.} \right) .$$

Within OBCs we thus have the following matrix representation

$$\mathbb{H} = \begin{pmatrix} 0 & v & & & & \\ v & 0 & w & & & \\ & w & 0 & v & & \\ & v & 0 & w & & \\ & w & 0 & v & & \\ & & & \ddots & \ddots & \ddots \\ & & & w & 0 & v \\ & & & v & 0 & 0 \end{pmatrix},$$

which is of dimension $2N \times 2N$ (for a chain of N unit cells) and is conveniently diagonalized numerically.

Eigenvalues and Eigenvectors

In this section we present the solutions of the eigenvalue problem for the matrix defined above, for different values of v and w . In particular, we fixed $w = 1$ as the energy scale and we varied v within the interval $[0, 2]$. In Figures 4, 5, 6 we show the resulting energy bands (left panels).

We notice that in all cases, the spectrum is perfectly symmetric with respect to $E = 0$ axis. This is a consequence of the presence of the *chiral symmetry* defined by:

$$\Gamma = P_A - P_B$$

where P_A, P_B are the projectors on the two sublattices A and B.

Γ and H anti-commute, $\{H, \Gamma\} = 0$, thus applying Γ to an eigenstate $|n\rangle$ with energy E_n we get an eigenstate with opposite energy:

$$H\Gamma|n\rangle = -\Gamma H|n\rangle = -E_n\Gamma|n\rangle ,$$

i.e. the particle-hole symmetry observed in the spectrum.

In light of the general concept of bulk-boundary correspondence, we may expect the presence of edge states in the non-trivial topological phase, exponentially localized at one side of the chain.

It can be shown, by looking for zero-energy solutions of the eigenvalue problem, that the edge states of this simple model have a vanishing energy, rapidly approaching zero in the limit of large N .

Because of this simple analytical argument, we compute the eigenstates with minimum absolute value of the energy (closest to the atomic energy), whose amplitudes are shown in the right panels of Figures 4, 5, 6. We can regard these states, assuming half filling, as the HOMO and LUMO states. They show an evident edge character when the winding number is nonzero ($v < w$), and become regular bulk states as the gap closes ($v = w$) and reopens with zero winding number ($v > w$).

A natural question is how to give a more quantitative definition of edge state, rather than a simple qualitative inspection. We propose the following: we define an edge state as a state s.t. the integrated charge density within the first (or last) fixed number $M \ll N$ of atomic sites is unchanged if we increase the total number of sites N . This definition captures the concept of exponential localization. We will refer to this quantity as the *edge charge* of the system. An example of edge states that perfectly satisfy this definition is shown in Fig. 3.

Let us now go in more detail, by sketching the analytical argument proving the existence of a pair of edge states with vanishing energy in the topological phase, $0 < v < w$. For future convenience we define:

$$\xi^{-1} = -\ln\left(\frac{v}{w}\right) > 0 , \quad (1)$$

which we shall prove to be the localization length scale of the edge states.

Looking for an eigenvector $\{C_i\}$ of H with zero-energy, we get the system:

$$\begin{cases} vC_2 = 0 \\ vC_1 + wC_3 = 0 \\ wC_2 + vC_4 = 0 \\ \vdots \end{cases} \quad (2)$$

Arbitrarily setting $C_1 = 1$, we have:

$$C_1 = 1, \quad C_2 = 0, \quad C_3 = -\frac{v}{w}, \quad C_4 = 0, \quad C_5 = \left(-\frac{v}{w}\right)^2, \quad \dots$$

which is summarized as

$$C_{2n} = 0, \quad C_{2n+1} = (-1)^n e^{-n/\xi}. \quad (3)$$

On the other hand, the last equation in (2) is: $C_{2N-1} = 0$. This condition is consistent with (3) only in the limit $N \rightarrow \infty$ (so that: $e^{-N/\xi} \sim 0$).

Similar considerations hold true starting from the other end of the chain and fixing $C_{2N} = 1$: one finds

$$C_{2n} = (-1)^{N-n} e^{-(N-n)/\xi}, \quad C_{2n+1} = 0.$$

Therefore, in the thermodynamic limit, we expect to have two degenerate eigenstates at exactly zero energy.

In the case of finite N , we expect to have two states with an energy splitting exponentially small in N ($\Delta_N \sim e^{-N/\xi}$) because of the non-vanishing overlap between the two edge states. This is indeed what we observe in the simulations; moreover ξ is verified to be the characteristic length of confinement of the edge states around the two ends of the chain (see Figures 3, 4, 5, 6).

Furthermore, we note that, if $|n\rangle$ is an eigenstate at energy E_n , we have:

$$E_n = \langle n | H | n \rangle = -\langle n | \Gamma H \Gamma | n \rangle = \langle n | P_A H P_B | n \rangle + \langle n | P_B H P_A | n \rangle$$

thus an eigenstate can be entirely localized on one of the two sublattices *only if* its energy is 0 and, *vice versa*, zero energy eigenstates can be chosen to have support on one sublattice only.

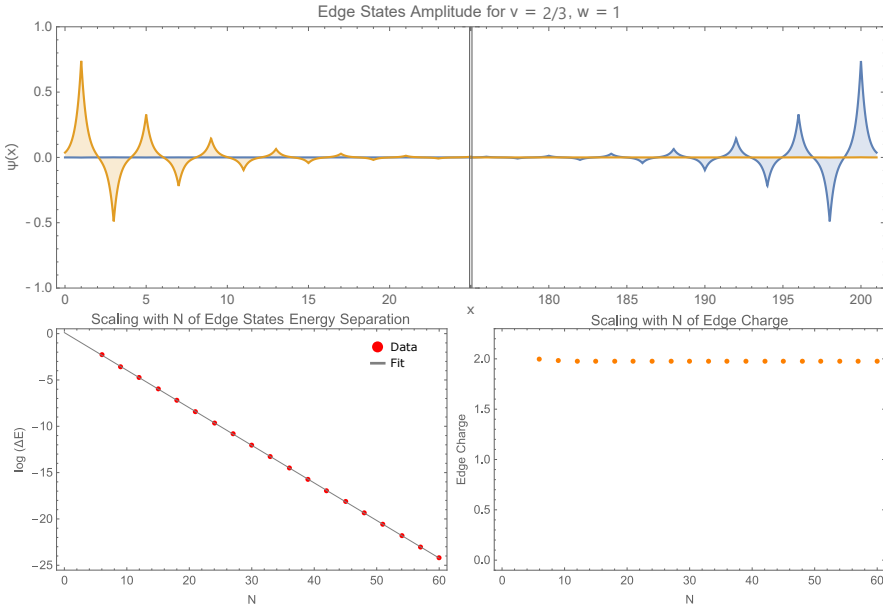


Figure 3: Top: Calculated amplitude of HOMO and LUMO levels, displayed in the relevant regions of the chain. Bottom: Chain-length dependence of energy splitting and sum of the edge charges of HOMO and LUMO levels.

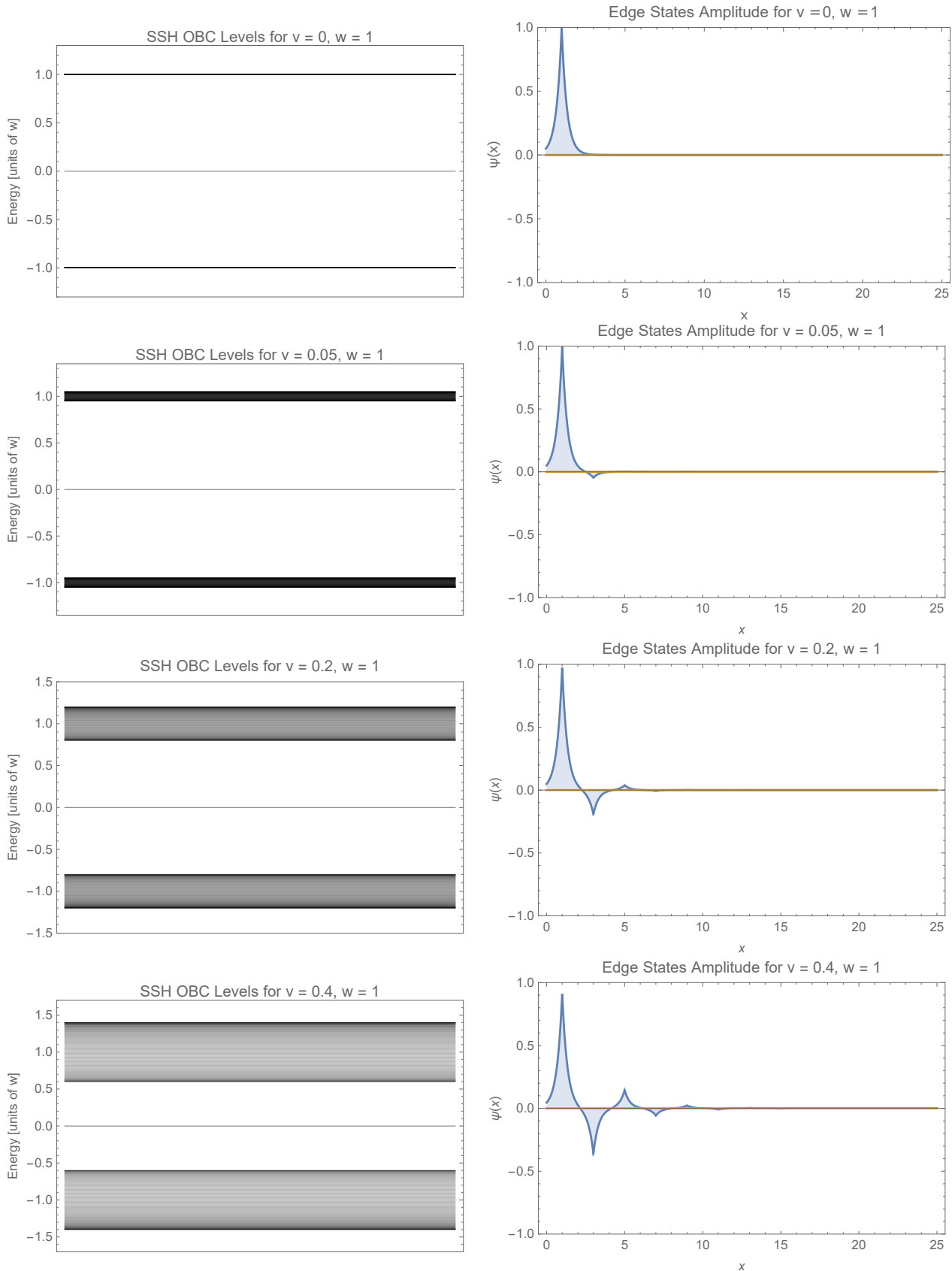


Figure 4: OBC Levels for the SSH Model, and corresponding HOMO and LUMO states. For simplicity, we show only the first part of the chain. Notice that in this region, in the topological phase, only one of the two edge states has non-zero amplitude.

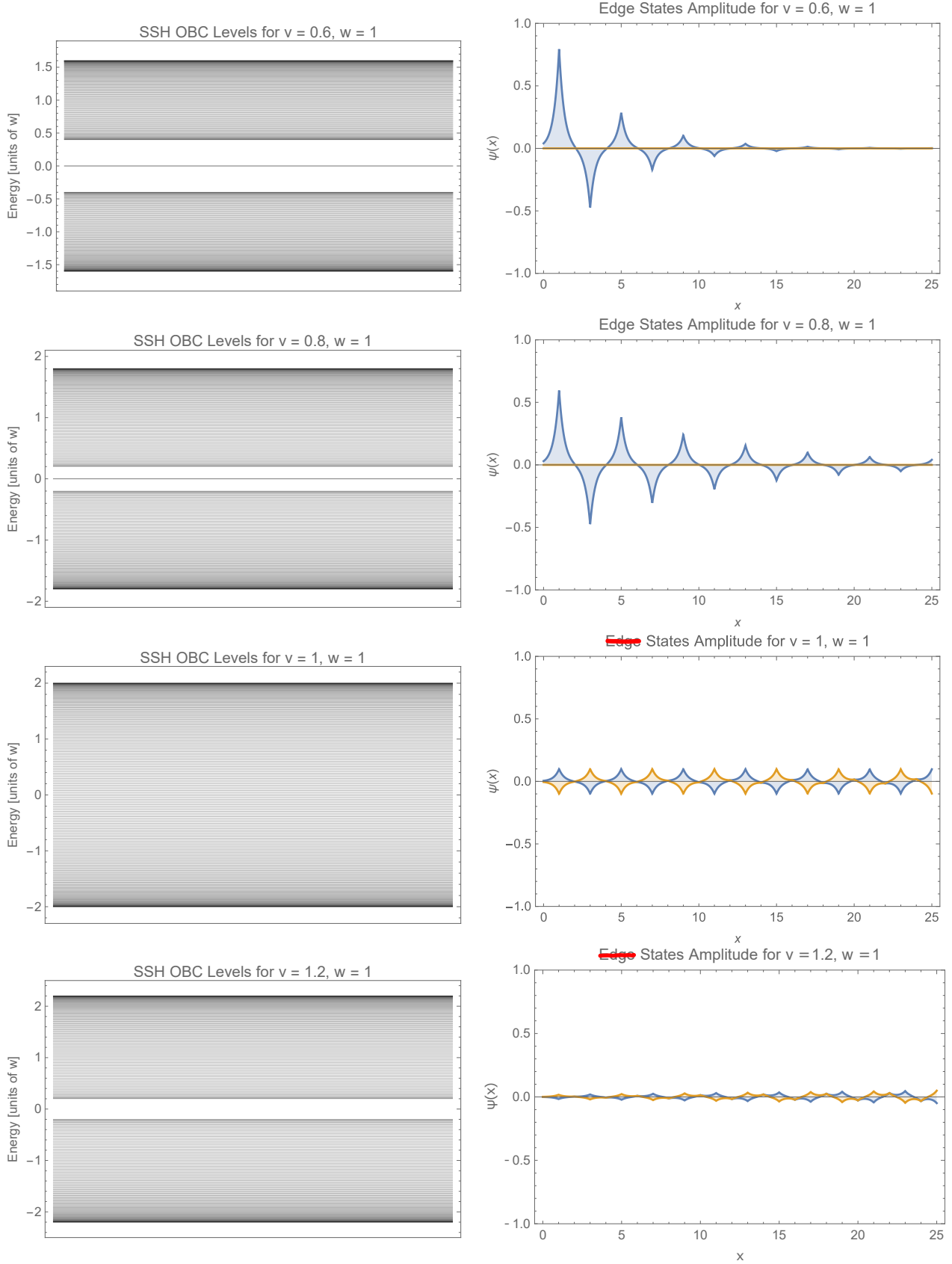


Figure 5: OBC Levels for the SSH Model, and correspondent HOMO and LUMO states. For simplicity, we show only the first part of the chain. Notice that in this region, in the topological phase, only one of the two edge states has non-zero amplitude

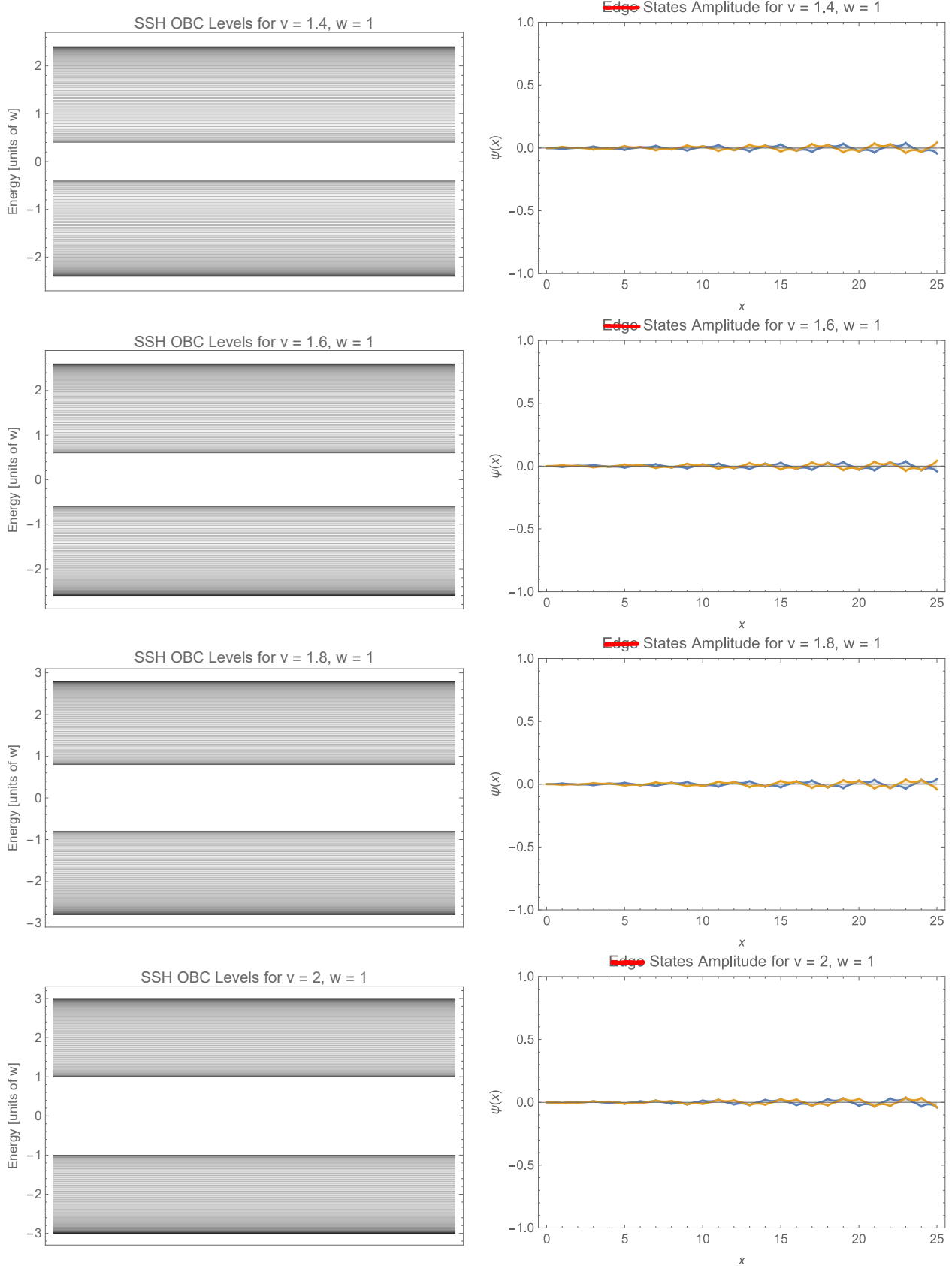


Figure 6: OBC Levels for the SSH Model, and correspondent HOMO and LUMO states. For simplicity, we show only the first part of the chain. Notice that in this region, in the topological phase, only one of the two edge states has non-zero amplitude.

Disorder

Now we consider a modified Hamiltonian in which we add some disorder to the hopping amplitudes. These disorder terms are random variables, uniformly distributed between $-R$ and $+R$. The “disorder strength” R is a parameter of choice for which we have spanned several values. We have of course focused on the “interesting” topological phase, fixing $w > v$.

The modified Hamiltonian reads:

$$\mathbb{H}_R = \begin{pmatrix} 0 & v + r_1 & & & \\ v + r_1 & 0 & w + r'_1 & & \\ & w + r'_1 & 0 & v + r_2 & \\ & & v + r_2 & 0 & w + r'_2 \\ & & & w + r'_2 & 0 & v + r_3 \\ & & & & \ddots & \ddots \\ & & & & & \ddots \\ & & & & w + r'_{n-1} & 0 & v + r_n \\ & & & & & v + r_n & 0 \end{pmatrix},$$

where $\{r_i, r'_i\} \in [-R, +R]$.

From the results of numerical diagonalization (Figures 7 and 8) we notice that:

- the chiral symmetry is maintained for all R values, as we expect since the inserted stochastic terms do not break the anticommutation of Γ and H ;
- the edge character of HOMO and LUMO states is well preserved at least until the gap remains open;
- the gap closes for $R > 2(w - v)$, i.e. for values of the disorder greater than the gap between the two bands of the SSH model in absence of disorder;
- for larger values of R , we still see localization at the edges. However, it is not clear whether it is imposed by topology or by disorder itself. Again referring to Figure 2, we see that with a closed gap the winding number (i.e. the topology of the system) is ill defined;¹
- for $R > w$ we finally see a gradual (and stochastic of course) breaking of the edge character.

In conclusion we can state that the chiral symmetry *protects* the edge character of HOMO and LUMO states against disorder on the v and w hoppings, for disorder strengths that preserve the topological phase of the system, i.e. small enough not to close the gap. The behavior of these zero energy states for larger values of disorder is unclear, since some localization can be due to disorder itself. However, since the gap is closed, they are not topologically protected anymore with respect to small perturbations of the model.

¹This statement can be cast in a even more dramatic form, if we consider that the winding number can be computed as the Berry phase of the eigenstates along the Brillouin Zone, so the presence of a closed gap in between breaks the adiabatic approximation and makes impossible to really define a Berry phase along the path.

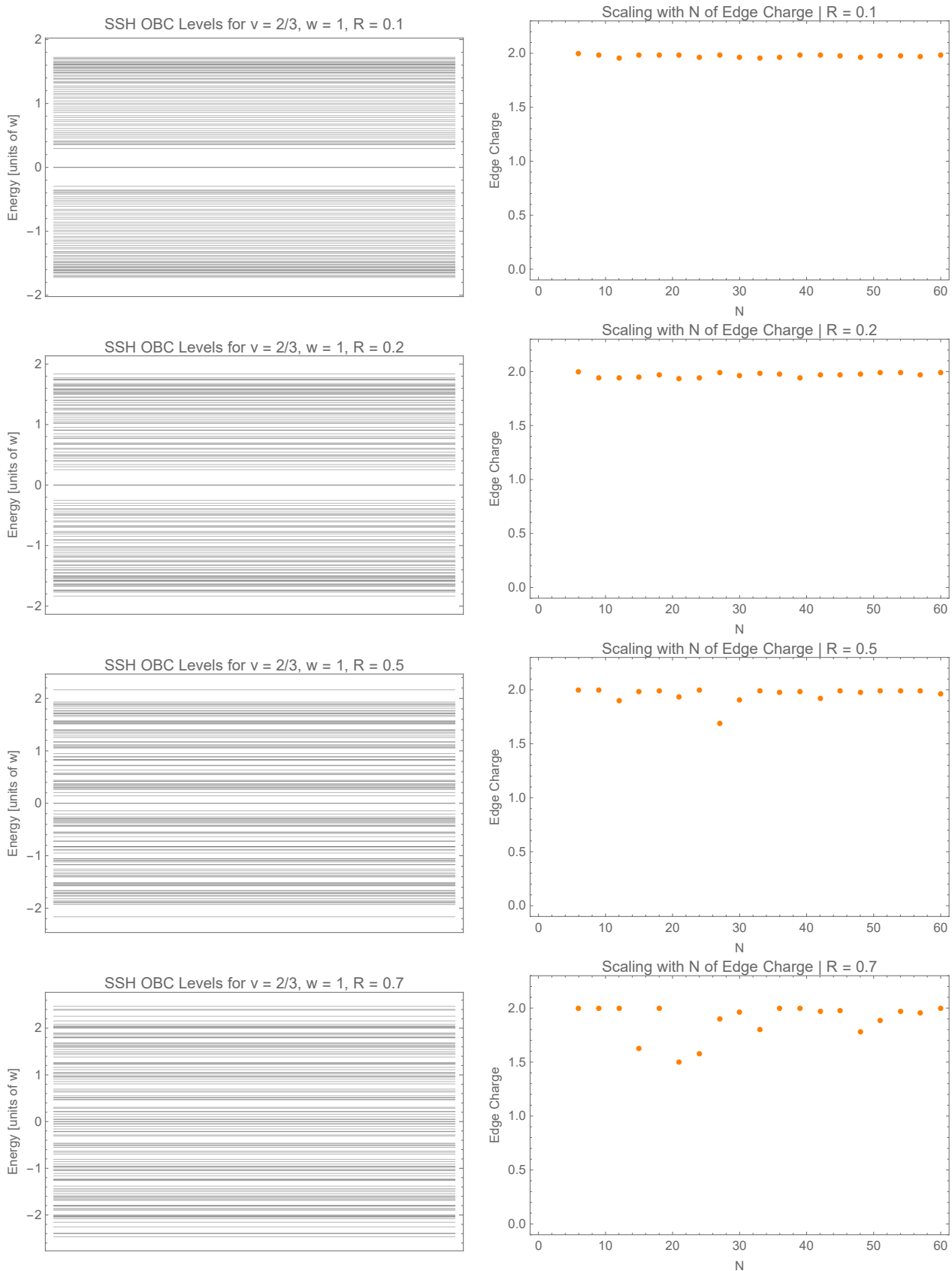


Figure 7: OBC Levels for the disordered SSH Model, and correspondent edge charge scaling.

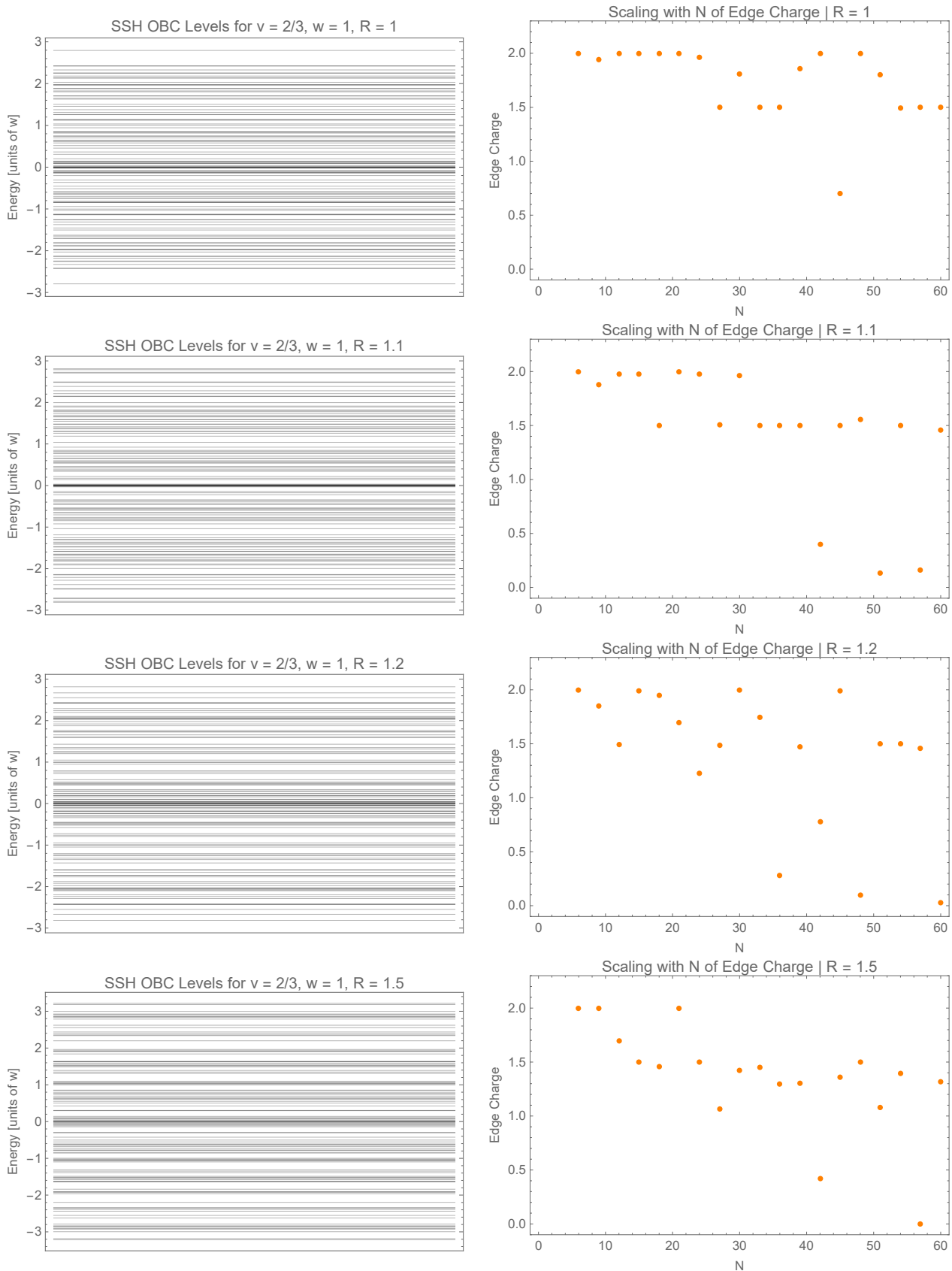


Figure 8: OBC Levels for the disordered SSH Model, and correspondent edge charge scaling.

More Neighbors

We now insert N.N.N. hoppings, assumed to be equal for both sublattices (see Figure 1): $v' = w' =: t < v < w$.

The addressed OBCs Hamiltonian matrix is then:

$$\mathbb{H}_{\text{N.N.N.}} = \begin{pmatrix} 0 & v & v' & & & \\ v & 0 & w & w' & & \\ v' & w & 0 & v & v' & \\ w' & v & 0 & w & w' & \\ v' & w & 0 & v & v' & \\ \ddots & \ddots & \ddots & \ddots & \ddots & \ddots \end{pmatrix} = \begin{pmatrix} 0 & v & t & & & \\ v & 0 & w & t & & \\ t & w & 0 & v & t & \\ t & v & 0 & w & t & \\ t & w & 0 & v & t & \\ \ddots & \ddots & \ddots & \ddots & \ddots & \ddots \end{pmatrix}.$$

The numerically computed energy schemes for fixed $v = 2/3$, $w = 1$ and increasing values of t are shown on the left panel of Figures 9, 10, 11. From the very first nonzero value of t , we see an evident breaking of the particle-hole symmetry and the reason is clear: the Hamiltonian connects different sites of the same sublattice, so we have $P_A H P_A \neq 0$ and $P_B H P_B \neq 0$, which implies that $\Gamma = P_A - P_B$ does not anti-commute anymore with H . As a result of this, the gap is not symmetric with respect to $E=0$, and the HOMO and LUMO energies are not located at the atomic energy anymore: thus some care is needed, in order to correctly select them among the computed eigenvectors².

On the right panel of Figures 9, 10, 11 is again displayed the edge charge, which:

- proves to be N -independent (edge-state-like) for t “small enough” with respect to $w/2$;
- initially decreases with N , and then assumes a constant value by further increasing the length of the chain (signature of “semi-edge-state”: edge states with a very long tail in the bulk) when we approach this upper limit: $t \lesssim w/2$;
- definitely breaks the edge character, dropping to zero for large enough N , for $t \geq w/2$.

These results seem reasonable, since the computed energy schemes show a gap closing, right at $t = w/2$: we would certainly expect to mix edge and bulk states from this point on. In conclusion, fixed N.N.N. hoppings do not degrade edge states *per se* (they disappear only at gap closing), but they do break chiral symmetry.

Disorder Again

Let us now consider again N.N.N. hoppings, but this time we shall assume them to be disordered, so the Hamiltonian matrix will be:

$$\mathbb{H}_W = \begin{pmatrix} 0 & v & t_1 & & & \\ v & 0 & w & t_2 & & \\ t_1 & w & 0 & v & t_3 & \\ t_2 & v & 0 & w & t_4 & \\ t_3 & w & 0 & v & t_5 & \\ \ddots & \ddots & \ddots & \ddots & \ddots & \ddots \end{pmatrix},$$

with $\{t_i\}$ uniformly distributed in the $[-W, W]$ interval (being W the N.N.N. disorder strength).

From our numerical results (see Figures 12 and 13) we conclude that:

- particle-hole symmetry is again manifestly broken in the spectrum, even for very small W values;
- edge character of HOMO and LUMO states is slightly more fragile in this case of disordered $\{t_i\}$ with respect to fixed t , so remarkably we destroy edge states *before* the gap closure;
- if compared to N.N. disorder, N.N.N. disorder is much more efficient in destroying edge states. This fact is a consequence of the breaking of the “protecting” chiral symmetry of the Hamiltonian.

²Essentially, we modified the code so as to sort the eigenstates by increasing energy, and we enumerated them from the lowest in energy to the highest. In this way, we simply selected the HOMO state, by knowing that the first band has $N - 1$ bulk states plus 1 “candidate edge” state. The next energy level corresponds to the LUMO state.

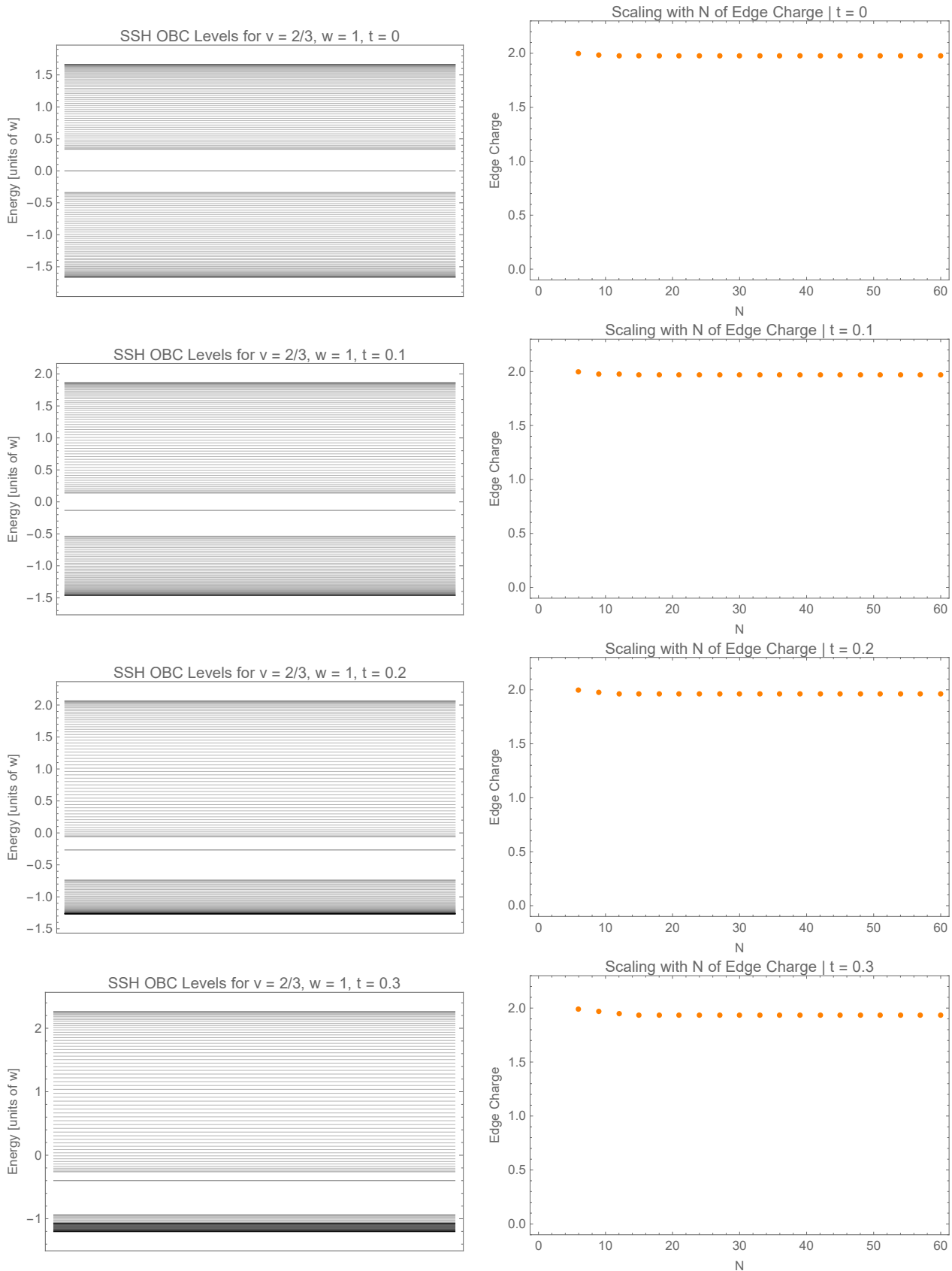


Figure 9: OBC Levels for the N.N.N. Extended SSH Model, and correspondent edge charge scaling.

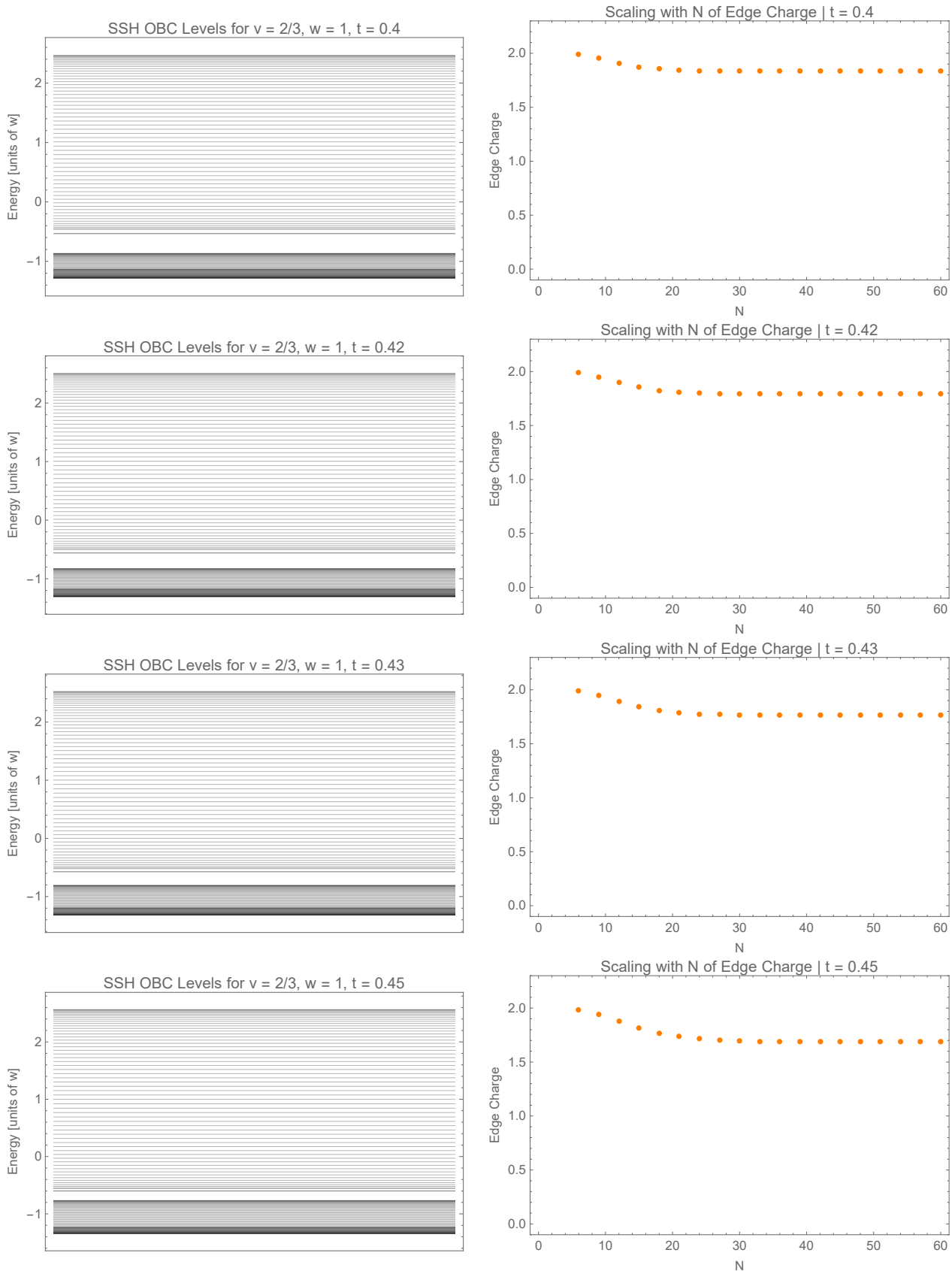


Figure 10: OBC Levels for the N.N.N. Extended SSH Model, and correspondent edge charge scaling.

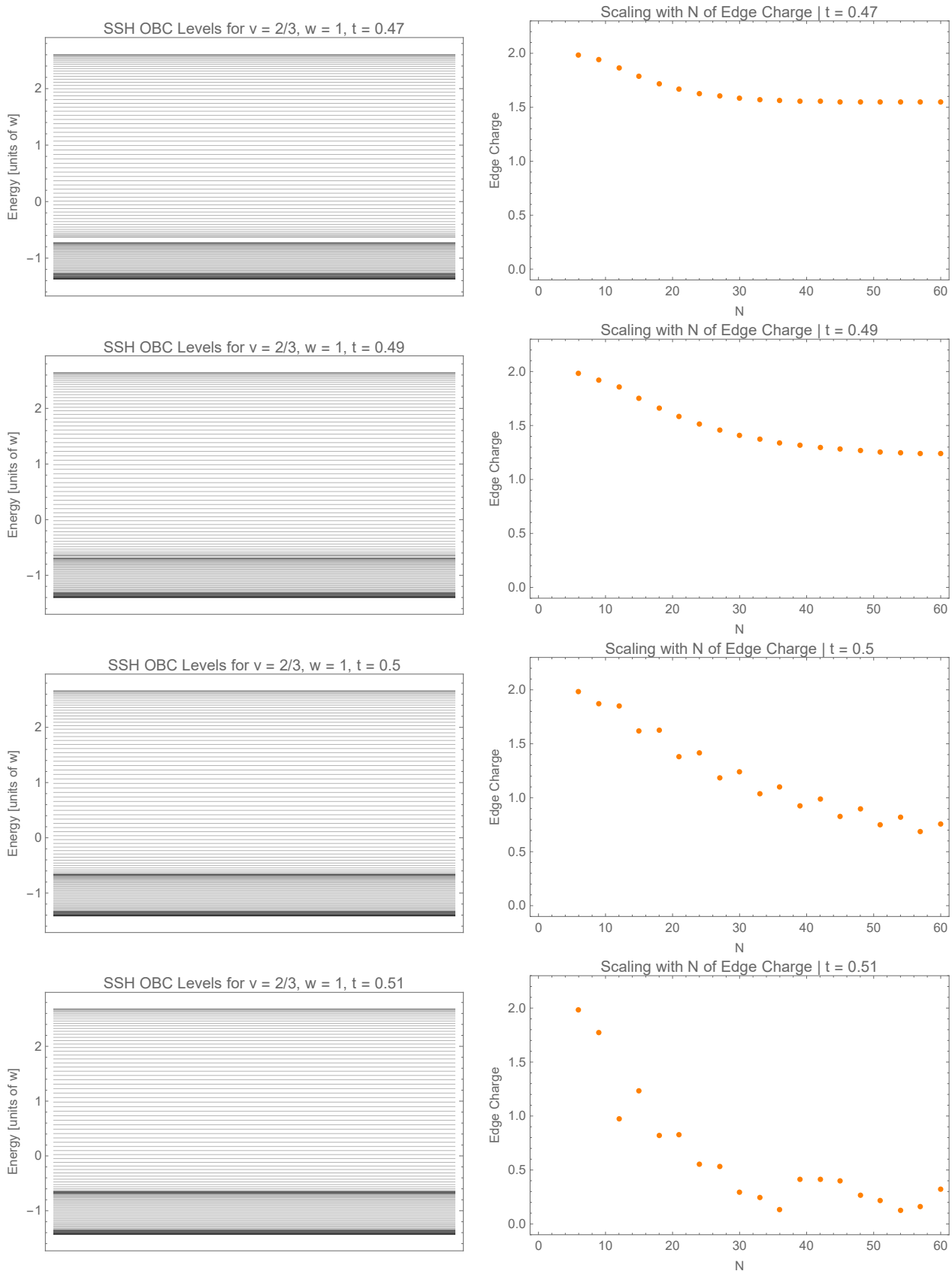


Figure 11: OBC Levels for the N.N.N. Extended SSH Model, and correspondent edge charge scaling.

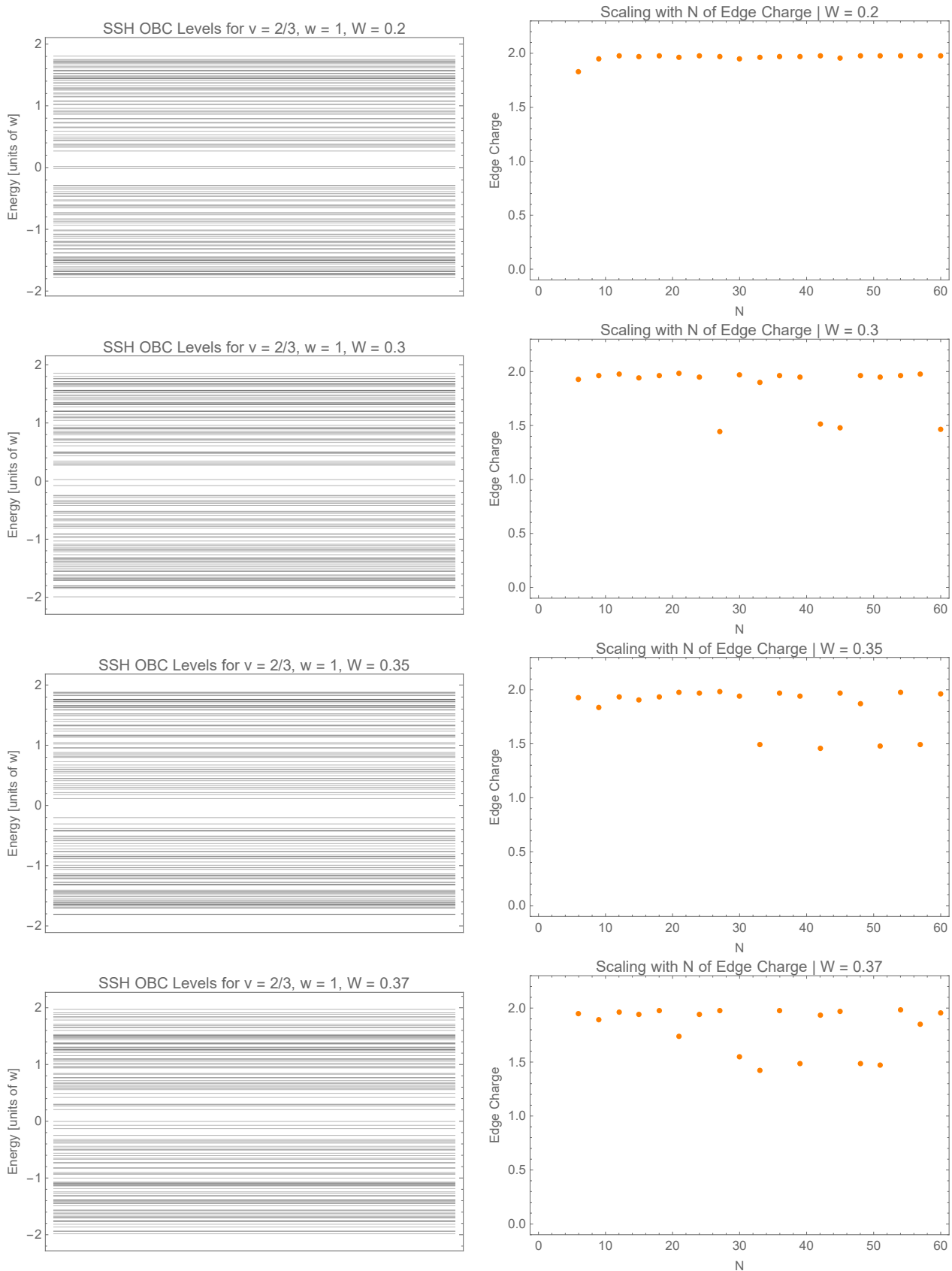


Figure 12: OBC Levels for the disordered N.N.N. Model, and correspondent edge charge scaling.

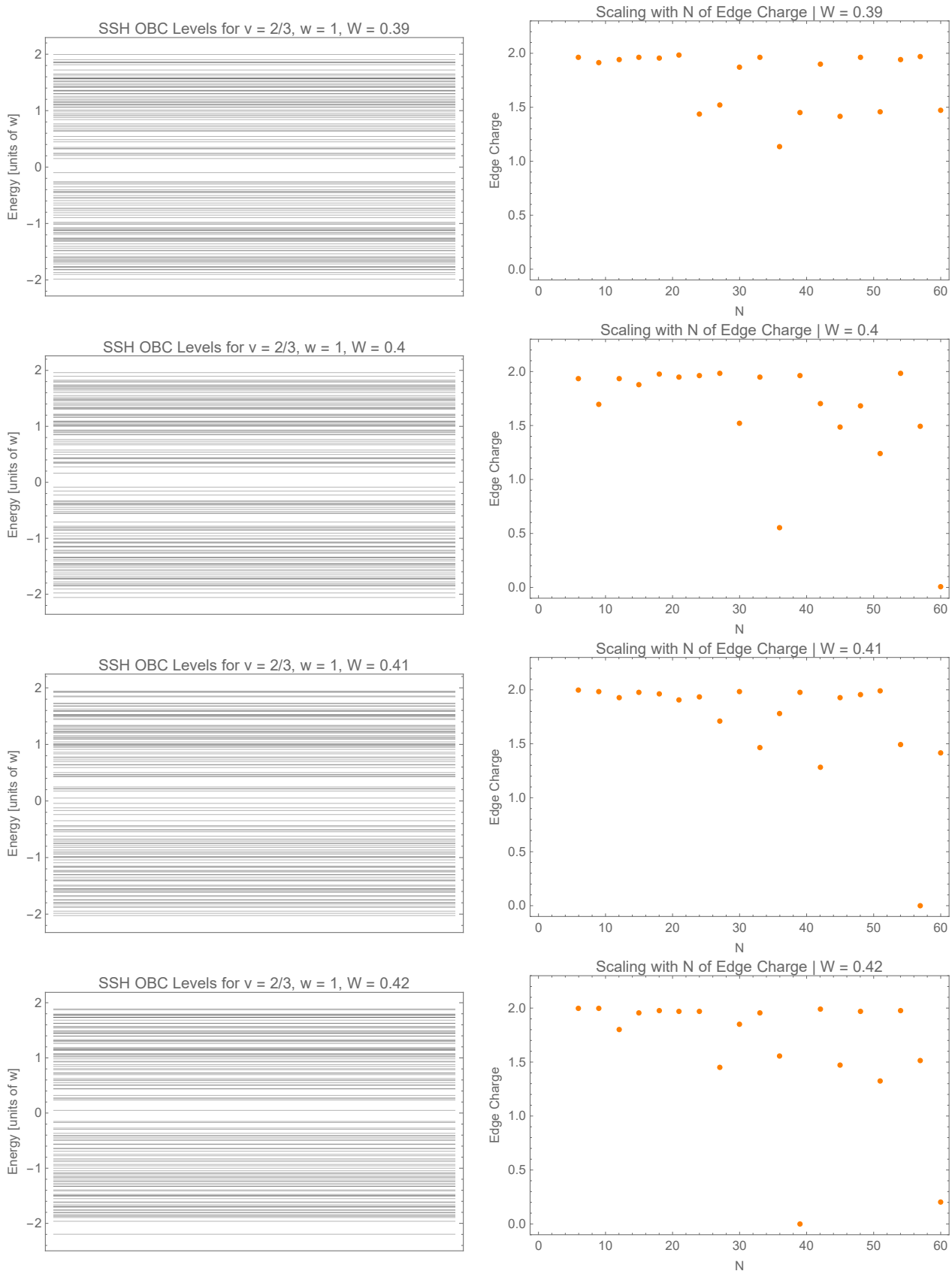


Figure 13: OBC Levels for the disordered N.N.N. Model, and correspondent edge charge scaling.

B1. Hofstadter-Harper Model

Let us consider a simple tight-binding model for non-interacting spinless fermions on a two-dimensional square lattice. By setting the on-site energies to zero, the Hamiltonian is given by:

$$H = - \sum_{i,j} \sum_{k,l} t_{(k,l) \rightarrow (i,j)} c_{ij}^\dagger c_{kl}, \quad t_{(k,l) \rightarrow (i,j)} = t \left(\delta_{ik} (\delta_{j+1,l} + \delta_{j-1,l}) + \delta_{jl} (\delta_{i+1,k} + \delta_{i-1,k}) \right),$$

where the indices i, k and j, l label respectively the x -coordinate and the y -coordinate on the lattice.

We want to consider this model with an external magnetic field $\mathbf{B} = B\hat{z}$ orthogonal to the lattice. How to change the Hamiltonian? A simple method is to observe that under an electromagnetic gauge transformation $\mathbf{A} \rightarrow \mathbf{A} + \nabla \Lambda(\mathbf{x})$, the creation/annihilation operators transform like the wave function in first quantization, namely:

$$\begin{cases} c_{ij}^\dagger \rightarrow e^{i \frac{e}{\hbar c} \Lambda(i,j)} c_{ij}^\dagger \\ c_{ij} \rightarrow e^{-i \frac{e}{\hbar c} \Lambda(i,j)} c_{ij} \end{cases},$$

and:

$$c_{ij}^\dagger c_{kl} \rightarrow e^{i \frac{e}{\hbar c} (\Lambda(i,j) - \Lambda(k,l))} c_{ij}^\dagger c_{kl}.$$

The theory must be gauge-invariant, therefore the transformation of the hopping amplitudes is:

$$t_{(k,l) \rightarrow (i,j)} \rightarrow e^{-i \frac{e}{\hbar c} (\Lambda(i,j) - \Lambda(k,l))} t_{(k,l) \rightarrow (i,j)}.$$

A meaningful choice (minimal coupling) is to set:

$$t_{(k,l) \rightarrow (i,j)} = t \left(\delta_{ik} (\delta_{j+1,l} + \delta_{j-1,l}) + \delta_{jl} (\delta_{i+1,k} + \delta_{i-1,k}) \right) \exp \left(-i \frac{e}{\hbar c} \int_{\mathbf{R}_{kl}}^{\mathbf{R}_{ij}} \mathbf{A} \cdot d\mathbf{r} \right)$$

in the presence of a magnetic field. By doing this $t_{(k,l) \rightarrow (i,j)}$ transforms as we want. The path of integration inside the exponential can be considered to be the lattice-bond that joins (k, l) and (i, j) ³. This substitution is usually called *Peierls substitution*. In our case a possible choice of the vector potential is:

$$\mathbf{A} = (0, Bx, 0) \quad (\text{Landau gauge}).$$

For future convenience we define:

$$t'(x) = t \exp \left(-i \frac{e}{\hbar c} Bx a \right) = t \exp \left(-2\pi i \frac{\Phi}{\Phi_0} \frac{x}{a} \right),$$

where a is the lattice spacing, $\Phi = a^2 B$ is the magnetic flux per plaquette and $\Phi_0 = (2\pi\hbar c)/e$ is the quantum of magnetic flux. We also define the ratio $\alpha = \Phi/\Phi_0$. Thus, we can write:

$$t_{(k,l) \rightarrow (i,j)} = \left(\delta_{ik} ((t'_i)^* \delta_{j+1,l} + t'_i \delta_{j-1,l}) + t \delta_{jl} (\delta_{i+1,k} + \delta_{i-1,k}) \right), \quad t'_i = t'(x = ia)$$

The resulting situation is depicted in Figure 14.

Bloch Theorem on \vec{x}

The original discrete translational invariance of the system along the \hat{x} -axis is broken by the dependence of hopping t' on the x -coordinate. Clearly, the discrete translational invariance on the y -coordinate still holds. However, if α is a rational number (i.e. $\alpha = P/Q$, with P, Q coprime integers) a supercell translational symmetry along x -coordinate is preserved. In fact:

$$t'(x + nQa) = t \exp \left(-2\pi i \frac{P}{Q} \frac{x}{a} - 2\pi i nP \right) = t \exp \left(-2\pi i \frac{P}{Q} \frac{x}{a} \right) = t'(x),$$

hence the system is still invariant under x -translations of a multiple of Qa . In this case, we can define a cell of length Qa in \hat{x} -direction and a in the \hat{y} -direction. In the case in which α is irrational, no periodicity can be found in x direction, and the unit cell will be a section of the lattice along \hat{x} , containing N_x atoms.

³This fact corresponds to assume that only one path contributes strongly in the path-integral calculation of the transition amplitude between the two sites.

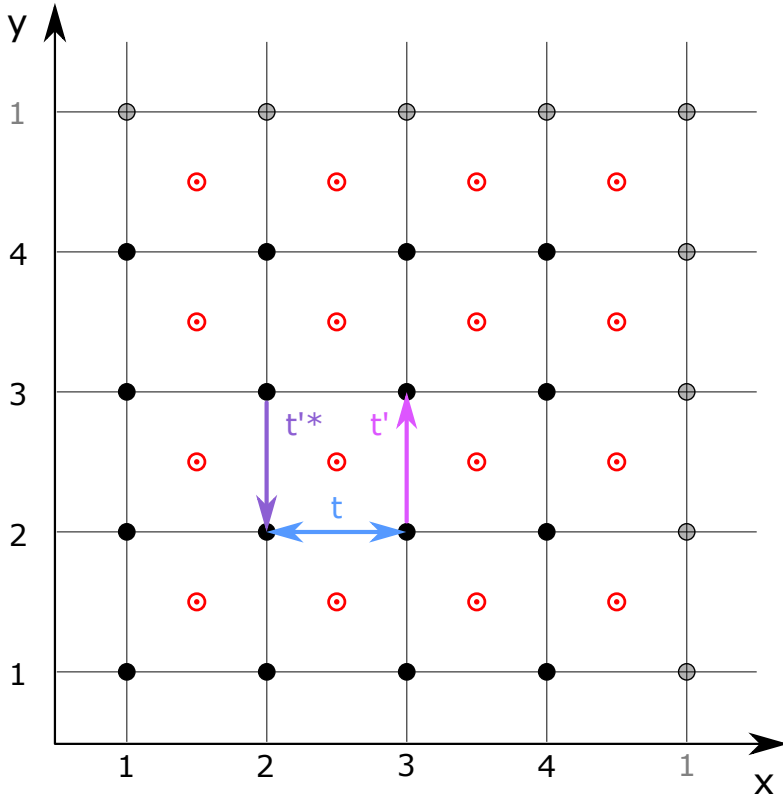


Figure 14: Schematic representation of the Hofstadter-Harper model. Red pointing-out-of-plane arrows correspond to the applied magnetic field and the in-plane arrows represent hopping amplitudes. Grey sites represent PBCs.

In any case, the system is still invariant under translations in the \hat{y} direction, therefore we can use Fourier transform:

$$c_{lm} = \frac{1}{\sqrt{N_y}} \sum_{k_y} e^{-ik_y ma} c_{lk_y}, \quad k_y = \frac{2\pi}{aN_y} k, \quad k = 0, 1 \dots N_y - 1$$

We get:

$$H = - \sum_{i,j} \sum_{k,l} \sum_{k_y, k'_y} \left(\delta_{ik} ((t'_i)^* \delta_{j+1,l} + t'_i \delta_{j-1,l}) + t \delta_{jl} (\delta_{i+1,k} + \delta_{i-1,k}) \right) \frac{1}{N_y} e^{ik_y ja} e^{-ik'_y la} c_{ik_y}^\dagger c_{ik'_y}$$

By using standard tricks, the first and the second terms become, respectively:

$$- \sum_{i,j} \sum_{k_y, k'_y} (t'_i)^* \frac{1}{N_y} e^{i(k_y - k'_y)ja} e^{-ik'_y a} c_{ik_y}^\dagger c_{ik'_y} = - \sum_i \sum_{k_y} (t'_i)^* e^{-ik_y a} c_{ik_y}^\dagger c_{ik_y},$$

and

$$- \sum_{i,j} \sum_{k_y, k'_y} t'_i \frac{1}{N_y} e^{i(k_y - k'_y)ja} e^{ik'_y a} c_{ik_y}^\dagger c_{ik'_y} = - \sum_i \sum_{k_y} t'_i e^{ik_y a} c_{ik_y}^\dagger c_{ik_y},$$

while the third and the fourth read:

$$- \sum_i \sum_{k_y, k'_y} t \frac{1}{N_y} e^{i(k_y - k'_y)ja} (c_{ik_y}^\dagger c_{i+1,k'_y} + c_{ik_y}^\dagger c_{i-1,k'_y}) = - \sum_i \sum_{k_y} t (c_{ik_y}^\dagger c_{i+1,k_y} + c_{i+1,k_y}^\dagger c_{ik_y}).$$

Finally, by using

$$(t'_j)^* e^{-ik_y a} + t'_j e^{ik_y a} = t (e^{2\pi i \alpha j} e^{-ik_y a} + e^{-2\pi i \alpha j} e^{ik_y a}) = 2t \cos(k_y a - 2\pi \alpha j),$$

we get:

$$H = - \sum_{k_y} \sum_i t \left(2 \cos(k_y a - 2\pi \alpha i) c_{ik_y}^\dagger c_{ik_y} + (c_{ik_y}^\dagger c_{i+1,k_y} + c_{i+1,k_y}^\dagger c_{ik_y}) \right) = \sum_{k_y} H_{k_y}. \quad (4)$$

As we see, H has become a block matrix (there is no coupling between states with different values of k_y).

Some properties of the spectrum of H can be easily understood.

1. Let us define two sub-lattices of the original (real-space) lattice, namely the even and the odd sub-lattices:

$$\begin{aligned}\mathcal{E} &= \{(i, j) \text{ such that } (-1)^{i+j} = +1\} \\ \mathcal{O} &= \{(i, j) \text{ such that } (-1)^{i+j} = -1\}\end{aligned}$$

In case of OBC, the HH Hamiltonian only couples sites of different sub-lattices (namely, if a site belong to \mathcal{E} is only coupled with sites of \mathcal{O} , and *vice versa*). Therefore, defining the sub-lattices projectors $P_{\mathcal{E}}$ and $P_{\mathcal{O}}$, we have:

$$P_{\mathcal{E}}HP_{\mathcal{E}} = 0 \quad P_{\mathcal{O}}HP_{\mathcal{O}} = 0.$$

Also defining $\Gamma = P_{\mathcal{E}} - P_{\mathcal{O}}$, we observe that:

$$\begin{aligned}\Gamma H \Gamma &= -P_{\mathcal{E}}HP_{\mathcal{O}} - P_{\mathcal{O}}HP_{\mathcal{E}} = -HP_{\mathcal{O}} - HP_{\mathcal{E}} = -H \\ \{H, \Gamma\} &= 0,\end{aligned}$$

therefore Γ is a chiral symmetry. If we apply Γ to an eigenstate $|n\rangle$ of H with energy E_n we get an eigenstate with opposite energy (see SSH model section). Thus, the spectrum S of H is symmetric with respect to 0:

$$S(H(\alpha)) = -S(H(\alpha)).$$

In case of PBC, $\{H, \Gamma\} = 0$ only if the *number of lattice sites* (i.e. of atoms) in both directions is even (otherwise the last site has the same parity of the first).

2. Because of the invariance of the physical system under time-reversal and because the magnetic field is odd under this symmetry, we have:

$$S(H(\alpha)) = S(H(-\alpha)).$$

3. Because of the form of the function $t'(x)$:

$$t'(x = ja; \alpha) = t'(x = ja; \alpha + n) \quad n \in \mathbb{Z}$$

and thus:

$$S(H(\alpha)) = S(H(\alpha + n)) \quad n \in \mathbb{Z}.$$

4. The spectrum is bounded from both above and below: $S(H(\alpha)) \subset [-4t, +4t]$. In fact, let us consider a generic single-particle state, with k_y fixed:

$$|\psi\rangle = \sum_j a_j c_{jk_y}^\dagger |0\rangle$$

We have:

$$\begin{aligned}\|H_{k_y}\psi\|^2 &= t^2 \left\| \sum_{j,l} a_j \left(2 \cos(k_y a - 2\pi\alpha l) c_{lk_y}^\dagger c_{lk_y} + (c_{lk_y}^\dagger c_{l+1,k_y} + c_{l+1,k_y}^\dagger c_{lk_y}) \right) c_{jk_y}^\dagger |0\rangle \right\|^2 = \\ &= t^2 \left\| \sum_j a_j \left(2 \cos(k_y a - 2\pi\alpha j) c_{jk_y}^\dagger c_{jk_y} + (c_{j-1,k_y}^\dagger c_{j,k_y} + c_{j+1,k_y}^\dagger c_{jk_y}) \right) c_{jk_y}^\dagger |0\rangle \right\|^2 = \\ &= t^2 \sum_j |(2a_j \cos(k_y a - 2\pi\alpha j) + a_{j+1} + a_{j-1})|^2 \|c_{jk_y}^\dagger |0\rangle\|^2 \leq \\ &\leq t^2 \sum_j (|2a_j \cos(k_y a - 2\pi\alpha j)| + |a_{j+1}| + |a_{j-1}|)^2 \leq \\ &\leq t^2 \sum_j (4|a_j|^2 + |a_{j+1}|^2 + |a_{j-1}|^2 + 4|a_j||a_{j+1}| + 4|a_j||a_{j-1}| + 2|a_{j-1}||a_{j+1}|) \leq 16t^2 \|\psi\|^2\end{aligned}$$

For the last inequality we used Cauchy-Schwarz:

$$\sum_j |a_j||a_{j+1}| \leq \left(\sum_j |a_j|^2 \right)^{1/2} \left(\sum_j |a_{j+1}|^2 \right)^{1/2} = \sum_j |a_j|^2 = \|\psi\|^2.$$

Given these observations, we can restrict ourselves to study $S(H(\alpha))$ in the range $\alpha = [0, 1/2]$. Another important result states that if α is irrational, then $S(H(\alpha))$ is a Cantor set, i.e. an infinite, closed, nowhere dense set with no isolated points (the so-called *Ten Martini Problem!*).⁴

If α is rational and equal to P/Q , the spectrum S is simply the union of Q bands. In this case we can define a unit cell of length Qa in the \hat{x} -direction. Using PBC, we can introduce Fourier transform also in this direction. It is convenient to change our notation, defining:

$$(c_{lk_y}^q)^\dagger, \quad c_{lk_y}^q$$

as the creation/annihilation operators acting on the site q of cell l^{th} . Obviously, q runs from 1 to Q , whereas l runs from 1 to N_x , where N_x is now redefined to be the *total number of cells* along \hat{x} . Let us remark that the total number of atoms along \hat{x} is now given by $N_x Q$. With this notation, the HH Hamiltonian is:

$$H = - \sum_{k_y} \sum_{i,q} t \left(2 \cos(k_y a - 2\pi\alpha q) (c_{ik_y}^q)^\dagger c_{ik_y}^q + ((c_{ik_y}^q)^\dagger c_{ik_y}^{q+1} + (c_{i,k_y}^{q+1})^\dagger c_{ik_y}^q) \right)$$

where: $c_{lk_y}^{Q+1} \equiv c_{l+1,k_y}^1$. We define also the Fourier transform:

$$c_{lk_y}^q = \frac{1}{\sqrt{N_x}} \sum_{k_x} e^{-ik_x l Q a} c_{k_x k_y}^q, \quad k_x = \frac{2\pi}{Q a N_x} k, \quad k = 0, 1 \dots N_x - 1.$$

By using this, we easily find that H is reduced to diagonal blocks labelled by k_x, k_y . The form of this block is given by:

$$(H_{k_x, k_y})_{qq'} = -t \left(2 \cos(k_y a - 2\pi\alpha q) \delta_{qq'} + \delta_{q,q+1} + \delta_{q,q-1} \right) \quad q, q' \in 2 \dots Q - 1$$

and:

$$(H_{k_x, k_y})_{11} = -2t \cos(k_y a - 2\pi\alpha) \quad (H_{k_x, k_y})_{QQ} = -2t \cos(k_y a - 2\pi\alpha Q) \\ (H_{k_x, k_y})_{1Q} = ((H_{k_x, k_y})_{Q1})^* = -te^{ik_x Q a}$$

To study the spectrum $S(H(\alpha))$ in PBC, we numerically diagonalized the $Q \times Q$ matrix H_{k_x, k_y} , with:

$$k_x \in [-\pi/(Qa), \pi/(Qa)] \quad k_y \in [-\pi/(Qa), \pi/(Qa)].$$

Note that k_y does not cover the whole Brillouin Zone, i.e. $[-\pi/a, \pi/a]$. Nevertheless, these values of k_y yield all possible energies, and the ignored portion of the two-dimensional bands is a simple periodic image (along k_y -direction) of the one here considered. Indeed, by observing that

$$\cos \left(\left(k_y + \frac{2\pi P}{Qa} \right) a - 2\pi\alpha j \right) = \cos(k_y a - 2\pi\alpha(j-1)),$$

it is clear (looking back to the HH Hamiltonian in the form of Eq. 4) that the spectrum of H_{k_y} has an additional periodicity of $2\pi P/(Qa)$ in k_y . By combining this symmetry with the usual one of the Brillouin Zone, we can restrict to the interval $k_y \in [-\pi/(Qa), \pi/(Qa)]$. This fact can formally be seen by introducing the equivalence relation $k_y \sim k'_y$ iff $S(H(k_y)) = S(H(k'_y))$. Then we have

$$k_y \sim k_y + \frac{2\pi}{a} n \sim k_y + \frac{2\pi}{a} \frac{P}{Q} m.$$

The distance between the two closest non-coinciding elements in the equivalence class is

$$\frac{2\pi}{a} \frac{nQ - mP}{Q} \stackrel{!}{=} \frac{2\pi}{a} \frac{1}{Q}.$$

because the linear Diophantine equation $nQ - mP = 1$ admits a solution, thanks to the Bézout identity.

Hofstadter Butterfly

We computed the spectrum $S(H(\alpha))$ for some (rational) values of $\alpha \in [0, 0.5]$. In Figure 15 we plotted the resulting spectrum $S(H(\alpha))$. The gaps in this plot are white regions resembling four wings of a butterfly. This is the so-called *Hofstadter Butterfly*, an object that is known to have some *self-similarity features* (like a fractal).

⁴Ref. <https://arxiv.org/abs/0908.1093>

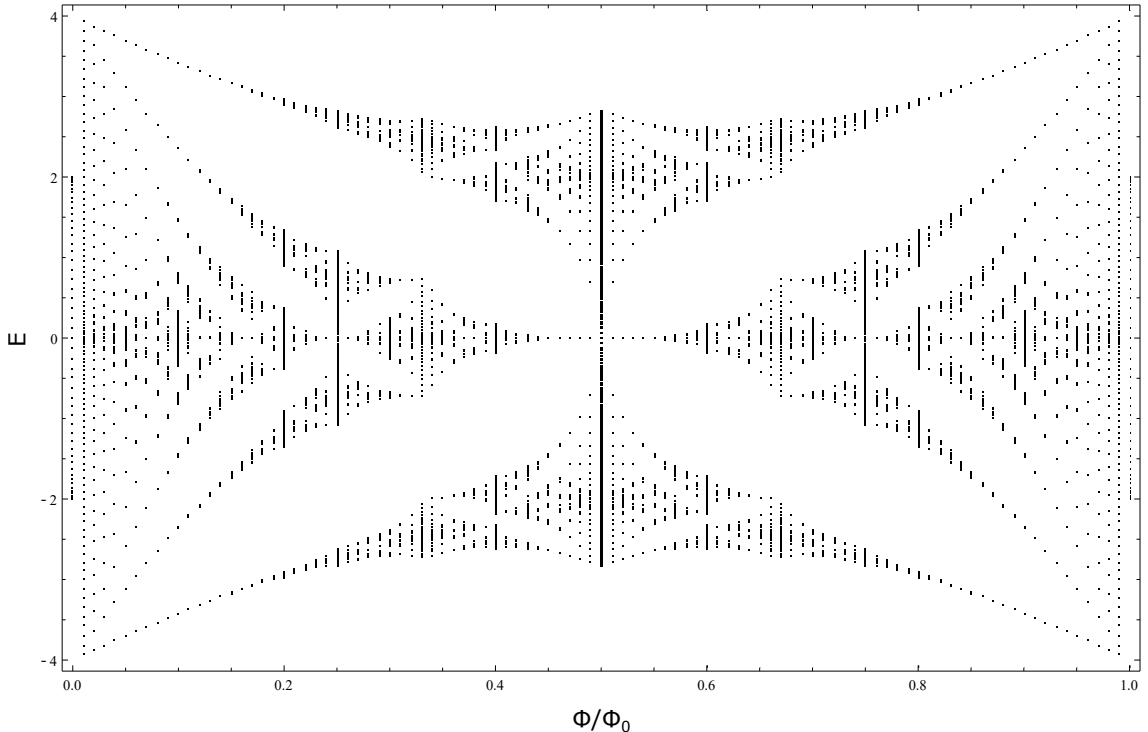


Figure 15: Hofstadter butterfly, obtained by considering a system of $N_x = N_y = 100$ cells in both the directions. The unit cell has Q atoms in the \hat{x} -direction and 1 atoms in the \hat{y} -direction. The values of α used are the integer multiples of $1/100$ (thus: $Q_{max} = 100$).

Edge States

Here we study the edge states for the case $\alpha = 1/3$, by using PBCs along \hat{y} -direction and OBCs along \hat{x} -direction. As a particular case of bulk-boundary correspondence, we expect that the opening of the boundary conditions along \hat{x} leads to the presence of topological edge states, located inside the band gaps.

As shown in Fig. 16, we observe the presence of a pair of edge states in each of the two band gaps. It can be shown that each pair of edge states is degenerate, respectively at $k_y = -2\pi/3$ and $k_y = \pi/3$. We numerically verified this result, which is visible in Fig. 16.

For the sake of definiteness, let us focus on the pair of edge states that are degenerate at $k_y = \pi/3$. Similar considerations clearly hold true for the other pair of edge states.

There are some subtleties in the correct definition of edge states, which are due to the crossing at the degeneracy point. For any k_y , we define the “high-energy” and “low-energy” states as the ones generating from the higher and lower bands (see the orange and red lines respectively, in Fig. 16).

We compute the left (right) edge charge for both this states by taking, as a reasonable measure of it, the sum of the square moduli of the wavefunction at the first (last) two sites.

The results are shown in Fig. 17 and 18. It is quite clear that the “high-energy” state is localized at the right side of the system, in a left k -space neighborhood of the crossing, $k_y \in (\pi/3 - \delta k, \pi/3)$, while it is localized at the left side of the system in a right k -space neighborhood $k_y \in (\pi/3, \pi/3 + \delta k)$. The opposite consideration is true for the “low-energy” state.

This clearly suggests to define the *physical* edge states by imposing that they vary smoothly with k_y at the crossing point, so they are localized either at the left or at the right edge, for any $k_y \in (\pi/3 - \delta k, \pi/3 + \delta k)$. These choice is clearly evidenced in the band structure in Fig. 19.

Consistently, the left and right edge charge for these two states vary smoothly, as shown in Figs. 20 and 21. We notice that for values of k_y sufficiently far away from the crossing point, the edge nature of these states is lost; the transition is gradual. As an example, in Figs. 22 and 23 we plot respectively the left and right edge states at the degeneracy point $k_y = \pi/3$ and for a slightly offset $k_y = \pi/3 + \delta k$ in Figs. 24 and 25.

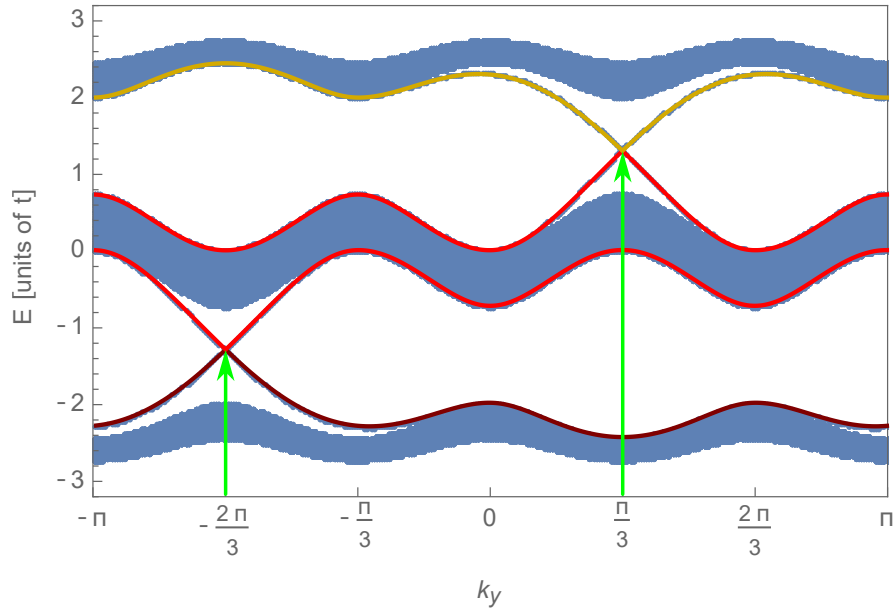


Figure 16: Band structure for the HH model in the case $\alpha = 1/3$, with PBC along \hat{y} -direction and OBC along \hat{x} -direction. The presence of topological edge states in the band gaps is evidenced through colors, as well as the points of degeneracy.

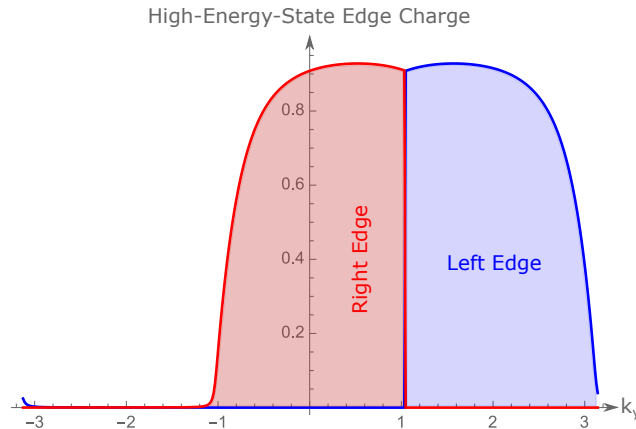


Figure 17: Right and left edge-charge of the edge state with higher energy, for k_y in a neighborhood of the crossing point at $\pi/3$.

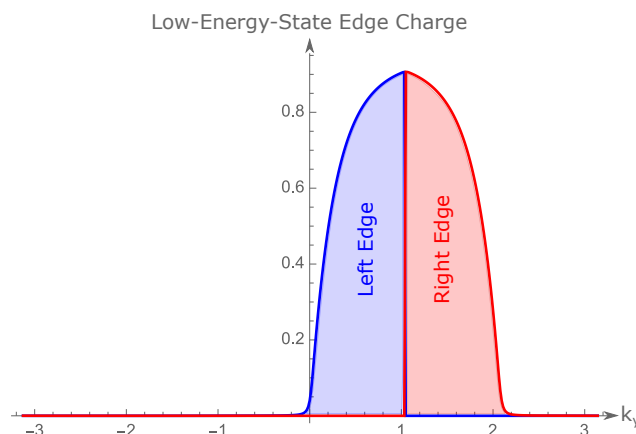


Figure 18: Right and left edge-charge of the edge state with lower energy, for k_y in a neighborhood of the crossing point at $\pi/3$.

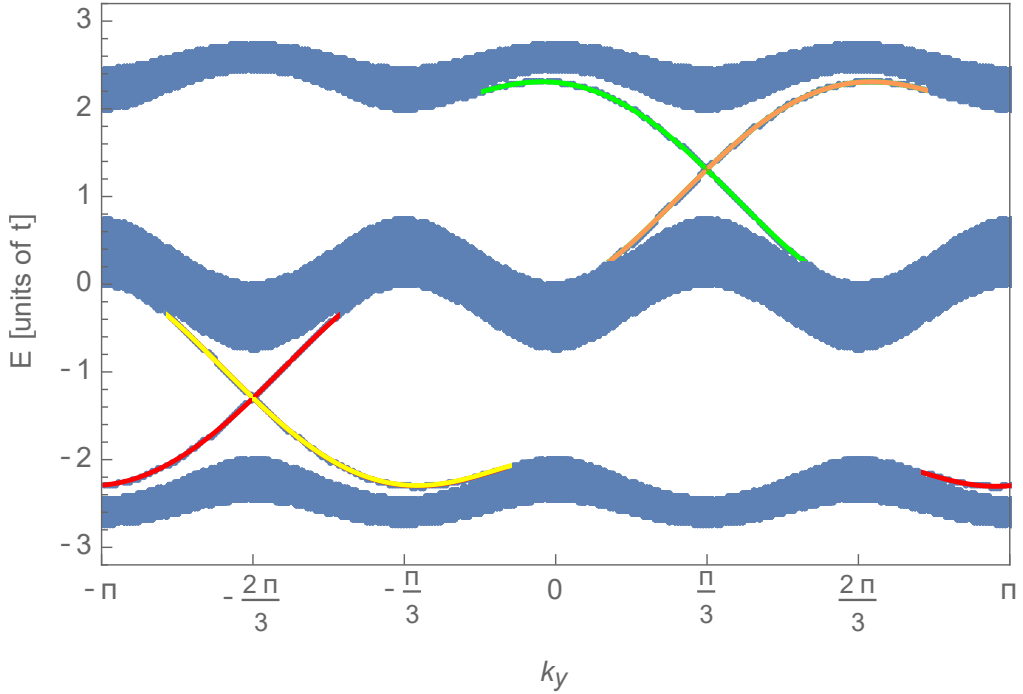


Figure 19: Band structure for the HH model in the case $\alpha = 1/3$, with PBCs along \hat{y} -direction and OBCs along \hat{x} -direction. The physical topological edge states are now evidenced through colors.

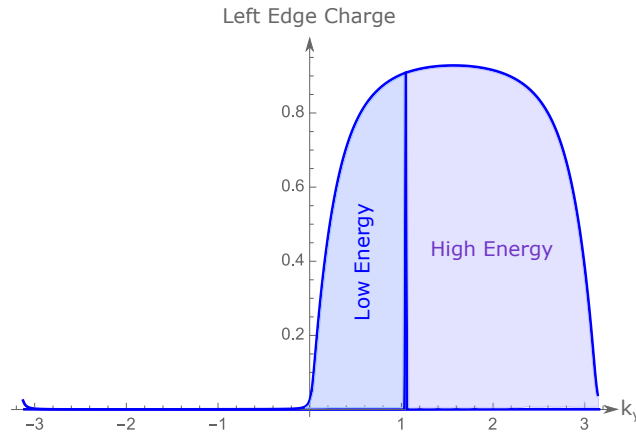


Figure 20: Left edge charge of the edge state localized at that side. Notice the regular behavior in a neighborhood of the crossing.

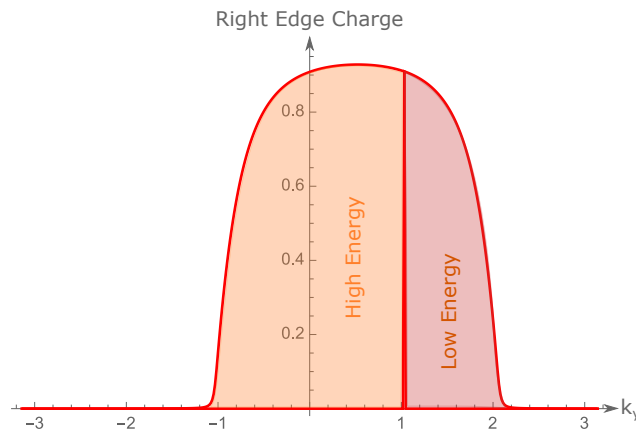


Figure 21: Right edge charge of the edge state localized at that side. Notice the regular behavior in a neighborhood of the crossing.

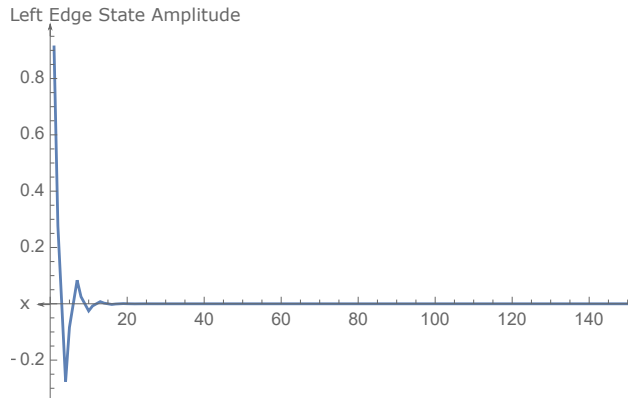


Figure 22: Left edge state at the degeneracy point $k_y = \pi/3$.

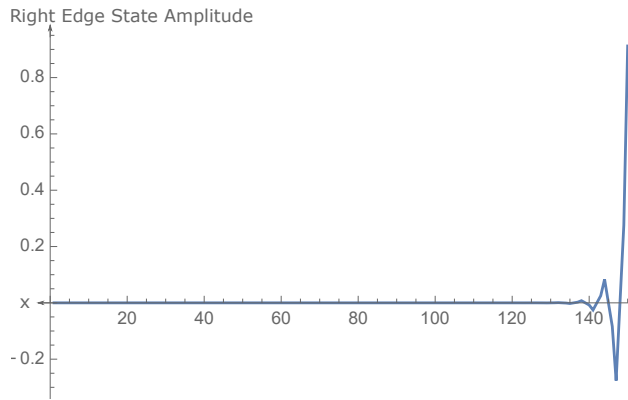


Figure 23: Right edge state at the degeneracy point $k_y = \pi/3$.

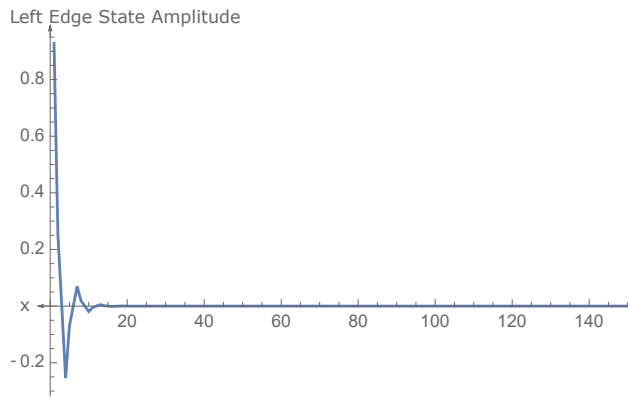


Figure 24: Left edge state at $k_y = \pi/3 + \delta k$.

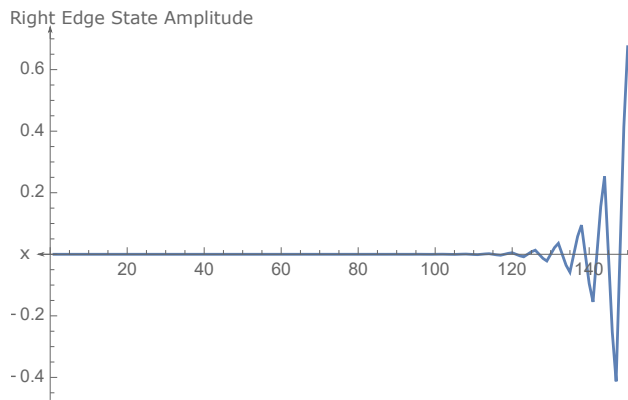


Figure 25: Right edge state at $k_y = \pi/3 + \delta k$.

In this particular case of $\alpha = 1/3$, we observe that the number of edge states of each band is equal to the modulus of its Chern number (see next section). However, this relation is not verified for other values of α . A simple relation between the Chern number of a band and the number of edge states is not observed, and we couldn't find a straightforward answer in the literature.

Note on robustness of edge states

Looking back at Eq. 4, we can slightly generalize the model by allowing two different values t_1 and t_2 , multiplying the diagonal and hopping terms respectively. One can show that by varying the ratio t_2/t_1 , the number of edge states that cross the gap, and the position of their degeneracies, is unaltered. This is shown in Fig. 26 for $t_2/t_1 = 0.2$.

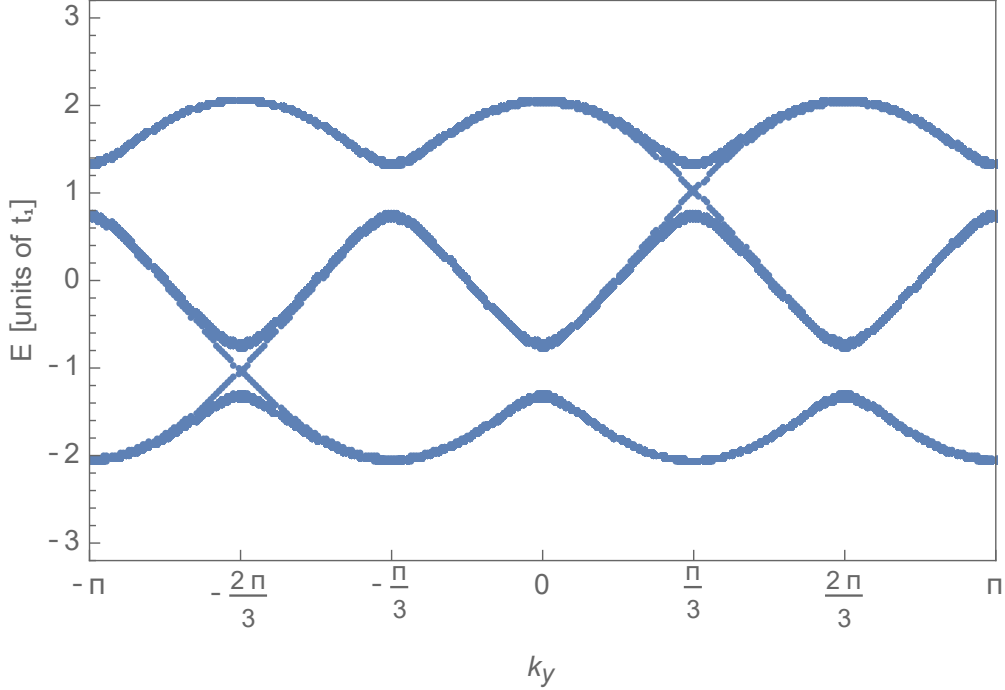


Figure 26: Analogous band structure for the *modified* HH model described in the text, in the case $t_2/t_1 = 0.2$. Note that, although the band structure changes, the topological states number and k -location are robust.

Chern Number

Our Brillouin-Zone is the subset

$$\text{BZ} = \left\{ k_x \in \left(-\frac{\pi}{Qa}, +\frac{\pi}{Qa} \right], k_y \in \left(-\frac{\pi}{a}, +\frac{\pi}{a} \right] \right\}$$

of \mathbb{R}^2 . The segment at $k_y = \pi/a$ is equivalent to that at $k_y = -\pi/a$, and the segment at $k_x = \pi/Qa$ is equivalent to that at $k_x = -\pi/Qa$. Thus the Brillouin-Zone has the topology of a two-dimensional torus:

$$\text{BZ} \simeq T^2 \simeq S^1 \times S^1.$$

For each point of the BZ, we have a set of Q eigenstates u such that:

$$H_{\mathbf{k}}^{\nu} u_{\mathbf{k}}^{\nu} = E^{\nu}(\mathbf{k}) u_{\mathbf{k}}^{\nu} \quad \nu = 1 \dots Q \quad \mathbf{k} = (k_x, k_y).$$

The energies $E^{\nu}(\mathbf{k})$ form the Q bands. It is always possible to apply a phase to an eigenvector, thus there is a “natural gauge transformation” of the $u_{\mathbf{k}}$, namely:

$$\tilde{u}_{\mathbf{k}}^{\nu} = e^{i\Lambda(\mathbf{k})} u_{\mathbf{k}}^{\nu}$$

The corresponding connection is:

$$\mathbf{A}^{\nu}(\mathbf{k}) = -i \langle u_{\mathbf{k}}^{\nu} | \nabla u_{\mathbf{k}}^{\nu} \rangle \quad (\text{Berry connection}).$$

Upon a gauge transformation, the Berry connection \mathbf{A} transforms as⁵

$$\tilde{\mathbf{A}}^\nu = \mathbf{A}^\nu + \nabla\Lambda.$$

The Berry curvature is defined as an anti-symmetric second-rank tensor associated to \mathbf{A} , namely:

$$\mathcal{B}_{ij}^\nu = \partial_i A_j^\nu - \partial_j A_i^\nu.$$

This object is gauge-invariant, and thus can be directly related to physical observables. Since we are on a two-dimensional manifold, there is only one independent component, that is:

$$\mathcal{B}_{xy}^\nu = -\mathcal{B}_{yx}^\nu = \partial_x A_y^\nu - \partial_y A_x^\nu \equiv B^\nu,$$

where we indicated with simplified notation $\partial_x \equiv \partial_{k_x}$ and $\partial_y \equiv \partial_{k_y}$. Note that $B^\nu = 1/2 \epsilon_{ij} \mathcal{B}_{ij}^\nu = \epsilon_{ij} \partial_i A_j^\nu$. The Chern number for the band ν is defined as:

$$C^\nu = \frac{1}{2\pi} \int_{T^2} \frac{dS_{ij}}{2} \mathcal{B}_{ij}^\nu(\mathbf{k}) = \frac{1}{2\pi} \int_{T^2} dk_x dk_y B^\nu(\mathbf{k}).$$

By the definition of \mathcal{B}_{ij}^ν , the previous integral is the flux on T^2 of the Berry curvature, which in turn is the curl of the connection (in mathematical language we are integrating the exterior derivative of a one-form on a two-dimensional manifold).

Naively, one could expect that $C^\nu = 0$ in all cases, just by applying Stokes' theorem and observing that a torus (being a closed surface) has no boundary ($\partial T^2 = \emptyset$). However this conclusion is false in general. In fact, even if $B^\nu(\mathbf{k})$ is regular on the whole Brillouin Zone, no one guarantees that also \mathbf{A} is regular. If \mathbf{A} has a singularity, then Stokes' theorem does not apply (see the standard case of a single spin 1/2).

For example, let us suppose to have only one singularity. We now split the torus into two disjoint subsets $(T^2)_I$ and $(T^2)_{II}$ such that the singularity is in $(T^2)_I$. We have:

$$C^\nu = \frac{1}{2\pi} \left(\int_{(T^2)_I} + \int_{(T^2)_{II}} \right) dk_x dk_y B^\nu(\mathbf{k})$$

In $(T^2)_{II}$ we can apply Stokes' theorem. On $(T^2)_I$, one must first find a gauge transformation such that $\tilde{\mathbf{A}}^\nu = \mathbf{A}^\nu + \nabla\Lambda$ is not singular in this region. Since the common boundary (a certain path γ) has opposite orientations in the two cases, the sum of the two integrals will be simply:

$$C^\nu = \frac{1}{2\pi} \oint \nabla\Lambda \cdot d\mathbf{r}.$$

This integral can be non-zero. In fact, there is no need to require that $\Lambda(\mathbf{k})$ is a single-valued function: the important thing is that $e^{i\Lambda(\mathbf{k})}$, which is the gauge phase factor, is single-valued! Thus the function $\Lambda(\mathbf{k})$ is locally (i.e. for any given \mathbf{k}) defined up to multiples of 2π . The usual argument for which the circulation has to be zero, holds true only for monodrome functions. In conclusion we get:

$$C^\nu \in \mathbb{Z}.$$

In the case of many singularities one can easily generalize this argument.

For a numerical computation of the Chern number, we made use of the following formula (refer to Figure 27):

$$C^\nu = -\frac{1}{2\pi} \sum_{\mathbf{k}} \text{Im} \left[\log \left(\langle u^\nu(k_x, k_y) | u^\nu(k_x + \delta_x, k_y) \rangle \langle u^\nu(k_x + \delta_x, k_y) | u^\nu(k_x + \delta_x, k_y + \delta_y) \rangle \langle u^\nu(k_x + \delta_x, k_y + \delta_y) | u^\nu(k_x, k_y + \delta_y) \rangle \langle u^\nu(k_x, k_y + \delta_y) | u^\nu(k_x, k_y) \rangle \right) \right], \quad (5)$$

where the sum is extended on a grid of plaquettes (i.e. small rectangles of size $\delta_x \times \delta_y$) partitioning the entire BZ. A crucial feature is that this formula preserves the gauge-invariance of C^ν , for any choice of the discrete grid covering the BZ. This is of primary importance, since the diagonalization routine assigns an erratic (random) phase factor to the eigenstates u^ν computed in each point of the grid.

Nevertheless, it is important to observe that this expression for the Chern number is still not uniquely defined. This is because the function $\text{Im}[\log(z)]$ is defined up to a multiple of 2π (or, equivalently, it is defined mod 2π).

⁵Note here the analogy with the vector potential of electromagnetism, both in the notation and in the transformation law. The same comment applies below for the Berry curvature.

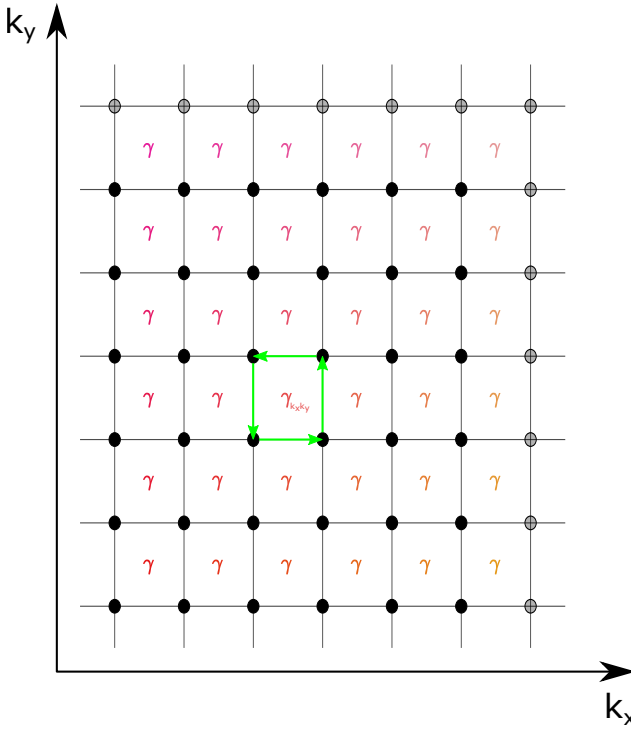


Figure 27: Brillouin Zone grid for the Chern number numerical computation, where the light dots are periodic images \mathbf{k} points at the BZ boundaries. The entire BZ is divided in small plaquettes, and we evaluate the Berry curvature flux upon each one by means of Stokes' theorem, i.e. by computing the 4-points Berry phase in its discretized version. The contribution γ of each plaquette can have a different (small) value, which is indicated graphically with a color scale. The total flux (the Chern number) is obtained by summing over the contributions of all plaquettes.

This implies that the expression in Eq. 5 for C^ν is defined mod 1, which is saying nothing, since the point is exactly to determine *which* integer equals the Chern number.

Before addressing the solution of this issue, we notice that the indeterminacy of mod 2π of each term of the sum is indeed expected, since the following term is nothing but the discretized expression for the Berry phase of a plaquette:

$$\gamma_{k_x, k_y} = -\text{Im} \left[\log \left(\langle u^\nu(k_x, k_y) | u^\nu(k_x + \delta_x, k_y) \rangle \langle u^\nu(k_x + \delta_x, k_y) | u^\nu(k_x + \delta_x, k_y + \delta_y) \rangle \right. \right. \\ \left. \left. \langle u^\nu(k_x + \delta_x, k_y + \delta_y) | u^\nu(k_x, k_y + \delta_y) \rangle \langle u^\nu(k_x, k_y + \delta_y) | u^\nu(k_x, k_y) \rangle \right) \right].$$

We know from the general theory of “Berryology” that the Berry phase is gauge-invariant only mod 2π . However, the Chern number formula has to be gauge-invariant. The natural question that arises is how to remove this mod 1 indetermination in Eq. 5.

An useful hint is found by taking the continuum limit $\delta_x, \delta_y \rightarrow 0$, finding:

$$C^\nu = -\frac{1}{2\pi} \sum_{\mathbf{k}} \text{Im} \left[\log \left((1 + i\delta_x A_x^\nu(k_x + \delta_x/2, k_y)) (1 + i\delta_y A_y^\nu(k_x + \delta_x/2, k_y + \delta_y/2)) \right. \right. \\ \left. \left. (1 - i\delta_x A_x^\nu(k_x + \delta_x/2, k_y + \delta_y)) (1 - i\delta_y A_y^\nu(k_x, k_y + \delta_y/2)) \right) \right] \simeq \\ \simeq -\frac{1}{2\pi} \sum_{\mathbf{k}} \text{Im} \left[\log \left(1 - i\delta_x \delta_y (\partial_y A_x^\nu - \partial_x A_y^\nu) \right) \right] \simeq \\ \simeq -\frac{1}{2\pi} \sum_{\mathbf{k}} \text{Im} \left[-i\delta_x \delta_y (\partial_y A_x^\nu - \partial_x A_y^\nu) \right] \simeq \frac{1}{2\pi} \sum_{\mathbf{k}} \delta_x \delta_y (\partial_y A_x^\nu - \partial_x A_y^\nu) \simeq \frac{1}{2\pi} \int_{T^2} dk_x dk_y B^\nu(\mathbf{k}).$$

The crucial point is that if the grid is sufficiently dense one must have a small value of the flux on each plaquette. Thus, the correct choice is to require that $\text{Im}[\log(z)] = \text{Arg}(z) \in (-\pi, \pi]$.

Equivalently, the correct formula for the Chern number C^ν is the same as Eq. 5, with $\log(z)$ replaced by $\text{Log}(z)$ (principal Logarithm). This is the formula we implemented in our code.

Incidentally, by using the equality mod 2π

$$\begin{aligned} \text{Arg} \left(\langle u^\nu(k_x, k_y) | u^\nu(k_x + \delta_x, k_y) \rangle \langle u^\nu(k_x + \delta_x, k_y) | u^\nu(k_x + \delta_x, k_y + \delta_y) \rangle \right. \\ \left. \langle u^\nu(k_x + \delta_x, k_y + \delta_y) | u^\nu(k_x, k_y + \delta_y) \rangle \langle u^\nu(k_x, k_y + \delta_y) | u^\nu(k_x, k_y) \rangle \right) = \\ \left(\text{Arg} \langle u^\nu(k_x, k_y) | u^\nu(k_x + \delta_x, k_y) \rangle + \text{Arg} \langle u^\nu(k_x + \delta_x, k_y) | u^\nu(k_x + \delta_x, k_y + \delta_y) \rangle \right. \\ \left. + \text{Arg} \langle u^\nu(k_x + \delta_x, k_y + \delta_y) | u^\nu(k_x, k_y + \delta_y) \rangle + \text{Arg} \langle u^\nu(k_x, k_y + \delta_y) | u^\nu(k_x, k_y) \rangle \right) \text{mod } 2\pi, \end{aligned}$$

and observing that, by summing over the grid points, all contributions cancel in pairs, this proves a remarkable result: the discretized formula for the Chern number gives the exact value, for any (sufficiently dense) grid in the BZ.

In the specific case of the HH model the Chern number can be computed analytically by means of the solutions of a first order Diophantine equation⁶:

$$\nu = Qs_\nu + Pt_\nu,$$

where s_ν, t_ν are integer variables. This equation has a unique solution for $\nu = 1 \dots Q$, with $|t_\nu| \leq Q/2$. Considering these solutions and conventionally defining $t_0 = 0$, then the Chern number of the ν^{th} band is given by:

$$C^\nu = t_\nu - t_{\nu-1}.$$

We wrote a code⁷ to solve the previous equation and found the Chern number associated to each band. There is perfect agreement between this analytical value and the numeric computation in terms of a BZ discretization.

As an example, we show in Fig. 28 the results for the numerical computation of the Chern number of the $\nu = 2$ band for the case $\alpha = 1/3$.

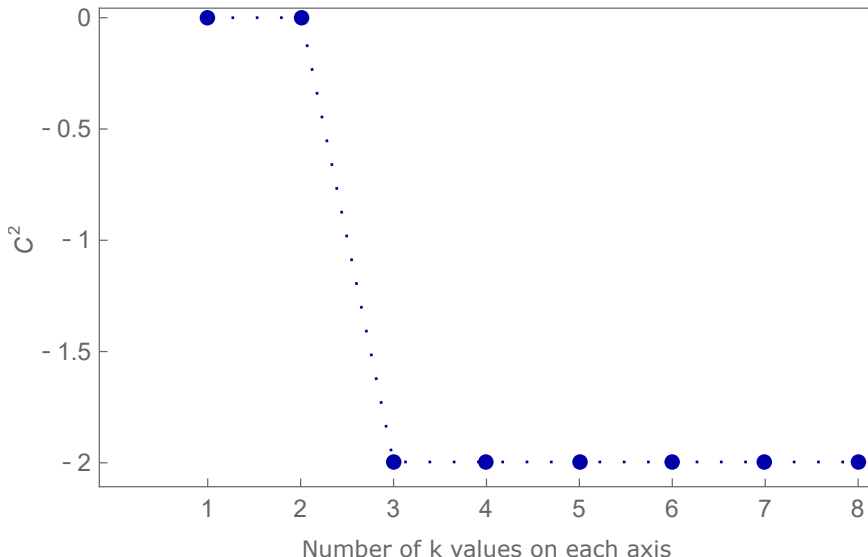


Figure 28: By increasing the number of points of the grid, one observes a rapid convergence to the theoretical value of the Chern Number.

⁶Ref. E. Fradkin: "Field Theories of Condensed Matter Physics", 2nd Edition

⁷Reported in Listing 6

MATHEMATICA Scripts

Listing 1: Mathematica script for SSH Model

```

1 Begin["omniaSSH`"];
2 ClearAll["omniaSSH`*"];
3 Clear[v1, w1, v2, w2, R, W, Ncells];
4
5 v1 = 2/3;
6 w1 = 1; (* Measure energy in units of w *)
7 v2 = 0;
8 w2 = v2;
9 RValues = {1.7}; (* List of n.n. disorder strengths *)
10 WValues = {0}; (* List of n.n.n. disorder strengths *)
11
12 NcellsValues =
13 Table[3 i , {i, 2,
14 20}]; (* List of numbers of unift cells *) (* Table[3i , {i,2,20}] *)
15 dEdgeValues =
16 Table[0 , {i, 1,
17 Length[NcellsValues]}]; (* List of energy differences between edge states *)
18 LeftChargeValues =
19 Table[0 , {i, 1,
20 Length[NcellsValues]}]; (* List of left edge charge values *)
21 RightChargeValues =
22 Table[0 , {i, 1,
23 Length[NcellsValues]}]; (* List of left edge charge values *)
24
25 PBC = False; (* PBC or OBC? *)
26 plotBands = False; (* Display plots of energy bands? *)
27 plotEdge = False; (* Display plots of edge states? *)
28 plotLinComb = False; (* Display plots of linear combinations of edge states? *)
29
30 (* Cycle on unit cells number *)
31 For[
32 k = 1, k <= Length[NcellsValues], k++,
33
34 (* Cycle on n.n. disorder strength R *)
35 For[
36 m = 1, m <= Length[RValues], m++,
37
38 (* Cycle on n.n.n. disorder strength W *)
39 For[
40 l = 1, l <= Length[WValues], l++,
41
42 Ncells = NcellsValues[[k]];
43 (*Print["\n\nNcells = ", Ncells,"\\n\\n"];*)
44
45 R = RValues[[m]];
46 (*Print["\\nR = ", R,"\\n"];*)
47
48 W = WValues[[l]];
49 (*Print["\\nW = ", W,"\\n"];*)
50
51 (* TB Hamiltonian Matrix *)
52 Hmatrix = SparseArray[
53 {
54 {i_, j_} /;
55 Abs[i - j] == 1 &&
56 If[i > j, Mod[i, 2] == 1, Mod[j, 2] == 1] -> w1,
57 {i_, j_} /;
58 Abs[i - j] == 1 &&
59 If[i > j, Mod[i, 2] == 0, Mod[j, 2] == 0] -> v1,
60 {i_, j_} /;
61 Abs[i - j] == 2 &&
62 If[i > j, Mod[i, 2] == 1, Mod[j, 2] == 1] -> v2,
63 {i_, j_} /;
64 Abs[i - j] == 2 &&
65 If[i > j, Mod[i, 2] == 0, Mod[j, 2] == 0] -> w2
66 }
67 , {2*Ncells, 2*Ncells}, 0];
68 Hmatrix = Normal[Hmatrix]; (* Reverting to dense matrix *)
69
70 (* Add PBC if present, with disorder already included *)
71 If[PBC,
72 Hmatrix[[1, 2*Ncells]] =
73 Hmatrix[[2*Ncells, 1]] = w1 + RandomReal[{-R, R}];
```

```

74 Hmatrix[[1, 2*Ncells - 1]] =
75   Hmatrix[[2*Ncells - 1, 1]] = v2 + RandomReal[{-W, W}];
76 Hmatrix[[2, 2*Ncells]] =
77   Hmatrix[[2*Ncells, 2]] = w2 + RandomReal[{-W, W}];
78 ];
79 (*MatrixForm[Hmatrix]*)

80
81 (* Disorder on n.n. hoppings *)
82 For[i = 1, i < 2*Ncells, i++, r = RandomReal[{-R, R}];
83   Hmatrix[[i, i + 1]] = Hmatrix[[i, i + 1]] + r;
84   Hmatrix[[i + 1, i]] = Hmatrix[[i + 1, i]] + r;
85 ];
86 (*MatrixForm[Hmatrix]*)

87
88 (* Disorder on n.n.n. hoppings *)
89 For[i = 1, i < 2*Ncells - 1, i++, r = RandomReal[{-W, W}];
90   Hmatrix[[i, i + 2]] = Hmatrix[[i, i + 2]] + r;
91   Hmatrix[[i + 2, i]] = Hmatrix[[i + 2, i]] + r;
92 ];
93 (*MatrixForm[Hmatrix]*)

94
95
96 (* Eigenthings *)
97 {En, Cn} =
98 Transpose[
99 Sort[Transpose[Eigensystem[Hmatrix]], #1[[1]] < #2[[1]] &]];
100

101 (* Energy Levels *)
102 plotEn[i_, x_] := En[[i]];
103 If[plotBands,
104 Print[Show[
105 Table[Plot[plotEn[i, x], {x, 0, 0.5},
106 PlotRange -> {Min[En] - 0.3, Max[En] + 0.3},
107 Axes -> {False, True},
108 PlotStyle -> {Black, Thickness[0.001], Opacity[0.3]},
109 Frame -> True, FrameTicks -> {None, Automatic},
110 FrameLabel -> {, "Energy [units of w]"},
111 PlotLabel ->
112 StringTemplate["SSH OBC Levels for v = `1`, w = `2`"][[v1,
113 w1]], {i, 1, 2*Ncells}]];
114 ];
115

116 (* Edge States *)
117 edge1 = Chop[Cn[[Ncells]]; (* We have sorted eigenvalues *)
118 edge2 = Chop[Cn[[Ncells + 1]]];
119 Enedge1 = En[[Ncells]];
120 Enedge2 = En[[Ncells + 1]];
121 dEnedge = Abs[Enedge1 - Enedge2];
122 (*Print["\n\nEnedge1 = ",Enedge1, "\n",Enedge2 = ",Enedge2, "\n",
123 "dEnedge = ",dEnedge, "\n"];*)
124
125 dEnedgeValues[[k]] = dEnedge;

126
127 (* Edge states *)
128 wfedge1[x_] :=
129 Sum[edge1[[n]]*Exp[-Abs[3*(x - n)]], {n, 1, 2*Ncells}];
130 wfedge2[x_] :=
131 Sum[edge2[[n]]*Exp[-Abs[3*(x - n)]], {n, 1, 2*Ncells};

132
133 edgeWeight1 =
134 Max[Sum[(edge1[[n]])^2, {n, 2*Ncells - 10, 2*Ncells}],
135 Sum[(edge1[[n]])^2, {n, 1, 10}]/
136 Sum[(edge1[[n]])^2, {n, 1, 2*Ncells}]];
(*Print["\n\nedgeWeight1 = ",edgeWeight1];*)

137
138 edgeWeight2 =
139 Max[Sum[(edge2[[n]])^2, {n, 2*Ncells - 10, 2*Ncells}],
140 Sum[(edge2[[n]])^2, {n, 1, 10}]/
141 Sum[(edge2[[n]])^2, {n, 1, 2*Ncells}]];
(*Print["\n\nedgeWeight2 = ",edgeWeight2];*)

142
143
144 If[plotEdge,
145 Print["\n\nEdge states\n"];
146 Print[
147 Plot[{wfedge1[x], wfedge2[x]}, {x, 0, 1/4*Ncells},
148 PlotRange -> {-1, 1}, Filling -> Axis, Frame -> True,
149 FrameLabel -> {x, \[Psi][x]}],
150

```

```

151 PlotLabel ->
152 StringTemplate["Edge States Amplitude for v = '1', w = '2'"][
153 v1, w1]];
154 Print[
155 Plot[{wfedge1[x], wfedge2[x]}, {x, 7/4*Ncells, 2*Ncells + 1},
156 PlotRange -> {-1, 1}, Filling -> Axis, Frame -> True,
157 FrameLabel -> {x, \[Psi][x]},
158 PlotLabel ->
159 StringTemplate["Edge States Amplitude for v = '1', w = '2'"][
160 v1, w1]];
161 ];
162
163 (* Linear combinations of edge states *)
164 linComb1[x_] :=
165 Sum[1/Sqrt[2] (edge1[[n]] + edge2[[n]])*Exp[-Abs[3*(x - n)]], {n,
166 1, 2*Ncells}];
167 linComb2[x_] :=
168 Sum[1/Sqrt[2] (edge1[[n]] - edge2[[n]])*Exp[-Abs[3*(x - n)]], {n,
169 1, 2*Ncells}];
170
171 edgeCombWeight1 =
172 Max[Sum[(edge1[[n]] + edge2[[n]])^2, {n, 2*Ncells - 10,
173 2*Ncells}], Sum[(edge1[[n]] + edge2[[n]])^2, {n, 1, 10}]]/
174 Sum[(edge1[[n]] + edge2[[n]])^2, {n, 1, 2*Ncells}];
175 (*Print["\n\nedgeCombWeight1 = ",edgeCombWeight1];*)

176
177 edgeCombWeight2 =
178 Max[Sum[(edge1[[n]] - edge2[[n]])^2, {n, 2*Ncells - 10,
179 2*Ncells}], Sum[(edge1[[n]] - edge2[[n]])^2, {n, 1, 10}]]/
180 Sum[(edge1[[n]] - edge2[[n]])^2, {n, 1, 2*Ncells}];
181 (*Print["\n\nedgeCombWeight2 = ",edgeCombWeight2];*)

182
183 If[plotLinComb,
184 Print["\n\nLinear combinations of edge states\n"];
185 Print[
186 Plot[{linComb1[x], linComb2[x]}, {x, 0, 1/4*Ncells},
187 PlotRange -> {-1, 1}, Filling -> Axis, Frame -> True,
188 FrameLabel -> {x, \[Psi][x]},
189 PlotLabel ->
190 StringTemplate["Edge States Amplitude for v = '1', w = '2'"][
191 v1, w1]];
192 Print [
193 Plot[{linComb1[x], linComb2[x]}, {x, 7/4*Ncells, 2*Ncells + 1},
194 PlotRange -> {-1, 1}, Filling -> Axis, Frame -> True,
195 FrameLabel -> {x, \[Psi][x]},
196 PlotLabel ->
197 StringTemplate["Edge States Amplitude for v = '1', w = '2'"][
198 v1, w1]];
199 ];
200
201 LeftCharge = Max[edgeWeight1, edgeCombWeight1];
202 (*Print["\n\nLeftCharge = ",LeftCharge]*);
203 LeftChargeValues[[k]] = LeftCharge;
204 (*Print["\n\nLeftChargeValues = ",LeftChargeValues]*);
205 RightCharge = Max[edgeWeight2, edgeCombWeight2];
206 (*Print["\n\nRightCharge = ",RightCharge]*);
207 RightChargeValues[[k]] = RightCharge;
208 (*Print["\n\nRightChargeValues = ",RightChargeValues]*);

209 ]
(* Cycle on W values CLOSING *)
210
211 ]
(* Cycle on R values CLOSING *)
212
213 ]
(* Cycle on unit cells number CLOSING*)

214
215
216
217 If[Length[NcellsValues] > 1,
218 Print["\n\n"];
219 (* Scaling of energy difference with N, we expect exponential decay *)
220
221
222
223 data = Table[{NcellsValues[[i]], dEnedgeValues[[i]]}, {i, 1,
224 Length[NcellsValues]}];
225 Print[ListLogPlot[data,
226 PlotLabel ->
227 "Scaling with N, Log plot of \[CapitalDelta]E(N)= exp(a N)",
```

```

228 AxesStyle -> Gray, PlotStyle -> {Red}]];
229
230 dataLog =
231 Table[{NcellsValues[[i]], Log[dEnedgeValues[[i]]]}, {i, 1,
232 Length[NcellsValues]}];
233 Print["\n"];
234 (* Linear fit: find a<0, where \[CapitalDelta]E(N)=exp(a N) *)
235 line[x_] = Fit[dataLog, {1, x}, x];
236 Print[Show[
237 ListPlot[dataLog,
238 PlotLabel -> "Scaling with N of Edge States Energy Separation",
239 Frame -> True, FrameLabel -> {"N", "log (\[CapitalDelta]E)" },
240 PlotStyle -> {Red}],
241 Plot[line[x], {x, 0, NcellsValues[[Length[NcellsValues]]]},
242 PlotStyle -> {Gray, Thickness[0.001]}]];
243
(* Scaling of Left Edge Charge with N, we expect it to be constant *)
244
245
246
247 dataLeft =
248 Table[{NcellsValues[[i]], LeftChargeValues[[i]]}, {i, 1,
249 Length[NcellsValues]}];
250 (*Print["\n\n"dataLeft = ",dataLeft];*)
251 dataRight =
252 Table[{NcellsValues[[i]]*0, RightChargeValues[[i]]}, {i, 1,
253 Length[NcellsValues]}];
254 (*Print["\n\n"dataRight = ",dataRight];*)
255 dataEdge = dataLeft + dataRight;
256 (*Print["\n\n"dataEdge = ",dataEdge];*)
257 Print[ListPlot[ dataEdge, PlotRange -> {-0.1, 2.3},
258 PlotLabel ->
259 StringTemplate["Scaling with N of Edge Charge | R = `1`"]<R>,
260 Frame -> True, FrameLabel -> {"N", "Edge Charge"}, PlotStyle -> Orange]];
261 ]
262
263
264 End[]];

```

Listing 2: Mathematica script for Computing HH Model Band Structure

```

1 Begin["HHBands`"];
2 ClearAll["HHBands`*"];
3
4 t = 1.;
5 Ncellsy = 90;
6 Ncellsx = 90;
7 \[Alpha] = 1/3;
8 Q = 3;
9 band1 = {};
10 band2 = {};
11 band3 = {};
12
13 MM = With[{Nn = N[Q]}, pattern = {t, t}],
14 SparseArray[{Band[{1, 2}, {-2, -1}] -> pattern,
15 Band[{2, 1}, {-1, -2}] -> pattern}, {Nn, Nn}]];
16 MM = Normal[MM];
17 NNN = IntegerPart[Ncellsy/3];
18 For[m = 0, m < NNN, m++, ky = 2*\[Pi]/Ncellsy*m - \[Pi];
19 For[n = 0, n < Ncellsx, n++, kx = 2*\[Pi]/(Q*Ncellsx)*n - \[Pi]/Q;
20 Matrix = Table[MM[[i]][[j]], {i, Q}, {j, Q}];
21 Matrix[[1, Q]] = Matrix[[1, Q]] + t*N[E^(-I*Q*kx)];
22 Matrix[[Q, 1]] = Matrix[[Q, 1]] + t*N[E^(+I*Q*kx)];
23 For[q = 1, q < Q + 1, q++,
24 Matrix[[q, q]] = 2*t*N[Cos[ky - 2*\[Pi]*\[Alpha]*q]];
(* Print[MatrixForm[Matrix]]; *)
25 \[Lambda] = Sort[Eigenvalues[Matrix]];
26 band1 = Append[band1, {kx, ky, \[Lambda][[1]]}];
27 band2 = Append[band2, {kx, ky, \[Lambda][[2]]}];
28 band3 = Append[band3, {kx, ky, \[Lambda][[3]]}];
29
30 ];
31 ];
32
33
34
35 p1 = ListPlot3D[band1, Mesh -> All, PlotRange -> All];
36 p2 = ListPlot3D[band2, Mesh -> All, PlotRange -> All];
37 p3 = ListPlot3D[band3, Mesh -> All, PlotRange -> All];
38 Show[p1, p2, p3]
39 Show[p1]
40 Show[p2]
41 Show[p3]
```

Listing 3: Mathematica script for Hofstadter Butterfly Rendering

```

1 Begin["Butterfly`"];
2 ClearAll["Butterfly`*"];
3
4 t = 1.;
5 Ncellsy = 5;
6 Ncellsx = 5;
7 \[Alpha]list = {}; (* Denser for nice butterfly, but beware: it will take time! *)
8 Qlist = {};
9 En = {};
10
11
12 For[kk = 1, kk < Length[\[Alpha]list] + 1, kk++,
13 \[Alpha] = \[Alpha]list[[kk]];
14 Q = If[\[Alpha] > 0, Denominator[Rationalize[\[Alpha]]], 1];
15 Print["Doing \[Alpha]= ", \[Alpha]];
16 Print["So Q is: ", Q];
17 Qlist = Append[Qlist, Q];
18 If[Q > 2,
19 MM = With[{Nn = N[Q]}, pattern = {t, t}],
20 SparseArray[{Band[{1, 2}, {-2, -1}] -> pattern,
21 Band[{2, 1}, {-1, -2}] -> pattern}, {Nn, Nn}],
22 If[Q == 2, MM = SparseArray[{1, 2} -> t, {2, 1} -> t}],
23 MM = {{0}}];
24 MM = Normal[MM];
25 En[\[Alpha]] = {};
26 For[m = 1, m < Ncellsy + 1, m++, ky = 2*\[Pi]/Ncellsy*m;
27 For[n = 1, n < Ncellsx + 1, n++, kx = 2*\[Pi]/(Q*Ncellsx)*n;
28 Matrix = Table[MM[[i]][[j]], {i, Q}, {j, Q}];
Matrix[[1]][[Q]] = Matrix[[1]][[Q]] + t*N[E^(-I*Q*kx)];
```

```

30 Matrix[[Q]][[1]] = Matrix[[Q]][[1]] + t*N[E^(+I*Q*kx)];
31 For[q = 1, q < Q + 1, q++,
32   Matrix[[q]][[q]] = 2*t*N[Cos[ky - 2*\[Pi]*\[Alpha]*q]];
33 (* Print[MatrixForm[Matrix]]; *)
34
35 If[Q > 1, En\[Alpha] = Append[En\[Alpha], Eigenvalues[Matrix]],
36 En\[Alpha] = Append[En\[Alpha], {Matrix[[1]][[1]]}]];
37
38 ];
39 ];
40
41 En = Append[En, En\[Alpha]];
42 ]
43 En;
44 Maxx = Max[En];
45 Minn = Min[En];
46
47
48 plotEn[x_, kk_, m_, n_, q_] :=
49 En[[kk]][[(m - 1) *Ncellsx + n]][[q]];
50
51
52 Enb = {};
53 For[kk = 1, kk < Length[\[Alpha]list] + 1, kk++,
54   Enb\[Alpha] = {};
55   For[m = 1, m < Ncellsy + 1, m++,
56     For[n = 1, n < Ncellsx + 1, n++,
57       For[q = 1, q < Qlist[[kk]] + 1, q++,
58         Enb\[Alpha] =
59           Append[Enb\[Alpha], {\[Alpha]list[[kk]],
60             En[[kk]][[(m - 1) *Ncellsx + n]][[q]]}];
61       ];
62     ];
63   ];
64 Enb = Append[Enb, Enb\[Alpha]];
65 ];
66
67 Show[
68 Table[ListPlot[Enb[[kk]],
69 PlotRange -> {{-0.1, 0.6}, {Minn - 0.2, Maxx + 0.2}}], {kk,
70 Length[\[Alpha]list]}]
71 ]

```

Listing 4: Mathematica script for OBCs HH Model

```

1 Begin["OBCHH`"];
2 ClearAll["OBCHH`*"];
3
4 a = 1; (*Unit of length*)
5 t = 1; (*For t\[NotEqual]1, the edge states for finite N have an \
6 avoided crossing*)
7
8 \[Alpha] = 1/3;
9 Q = If[\[Alpha] > 0, Denominator[Rationalize[\[Alpha]]], 1];
10
11 PBC = False; (* PBC or OBC? *)
12
13
14 (* Numbers of cells *)
15 Ncx = 50; (*40*)
16 Ncy = 420; (*300*)(*Should be divisible by 6, in order to get the \
17 points where edge states are degenerate*)
18 (* Numbers of atoms *)
19 Nax = Q Ncx;
20 Nay = Ncy;
21
22 (*Define NULL matrices*)
23 En = Table[0, {m, 1, Nay}, {l, 1, Nax}];
24 vv = Table[0, {m, 1, Nay}, {l, 1, Nax}];
25
26 (* Points of the BZ along y *)
27 time = Timing[
28   For[m = 1, m <= Nay, m++, ky = -\[Pi] + 2 \[Pi] m/Nay;
29
30   ClearAll[i, j];
31   Hmatrix = Normal[SparseArray[
32     {
33       {i_, j_} /; Abs[i - j] == 1 -> t,
34       {i_, j_} /; Abs[i - j] == 0 -> 2 Cos[ky a - 2 Pi \[Alpha] i]
35     }
36   , {Nax, Nay}, 0]];
37
38   If[PBC,
39     Hmatrix[[1, Nay]] = Hmatrix[[Nay, 1]] = t;
40   ];
41
42   eigen =
43   Transpose[
44     Sort[Transpose[Eigensystem[N[Hmatrix]]], #1[[1]] < #2[[1]] &]];
45
46 (*1d energy bands*)
47 For[l = 1, l <= Nax, l++,
48   En[[m, l]] = eigen[[1, l]];
49   vv[[m, l]] = eigen[[2, l]];
50 ]
51
52 ] (* Cycle on BZ CLOSING *)
53 ];
54
55 Print["\nTime for one eigenvalue/eigensystem evaluation ",
56 time[[1]]/(Nax*Nay)]
57
58 (*Plot of energy bands*)
59 Show[
60   Table[
61     ListPlot[Table[{-\[Pi] + 2 \[Pi] m/Nay, En[[m, l]]}, {m, 1, Nay}],
62       PlotRange -> {{-Pi, Pi}, {-3.2, 3.2}}, {l, 1, Nax}
63     ], Frame -> True,
64     FrameLabel -> {"\!\(\*\SubscriptBox[\(k\), \(y)]\)", "E [units of t2]"}, Axes -> False,
65     FrameTicks -> { {Automatic,
66       None} , {{-Pi, -2 Pi/3, -Pi/3, 0, Pi/3, 2 Pi/3, Pi}, None} }
67   ]
68
69
70 (*Points of degeneracy of the edge states, for t=1*)
71
72 (*Each of the three "bands" has the same number of state. Thus the \
73 position of edge states could be predicted a priori*)

```

```

75 indecesL = {}; (*positions of edge states at ky<0*)
76
77 For[l = 1, l <= Nax, l++,
78  If[-2 < En[[Nay/6, l]] < -1, AppendTo[indecesL, l]];
79 ]
80
81 indecesL
82 En[[Nay/6, indecesL[[1]]]]
83 En[[Nay/6, indecesL[[2]]]]
84
85
86 indecesR = {}; (*positions of edge states at ky>0*)
87
88 For[l = 1, l <= Nax, l++,
89  If[1 < En[[2 Nay/3, l]] < 2, AppendTo[indecesR, l]];
90 ]
91
92 indecesR
93 En[[2 Nay/3, indecesR[[1]]]]
94 En[[2 Nay/3, indecesR[[2]]]]
95
96
97 (*Edge states 1d dispersion relation*)
98 dispEdge1 =
99  Table[{-\[Pi] + 2 \[Pi] m/Nay, En[[m, indecesL[[1]]]], {m, 1, Nay}],
100 dispEdge2 =
101  Table[{-\[Pi] + 2 \[Pi] m/Nay, En[[m, indecesL[[2]]]], {m, 1, Nay}],
102 dispEdge3 =
103  Table[{-\[Pi] + 2 \[Pi] m/Nay, En[[m, indecesR[[1]]]], {m, 1, Nay}],
104 dispEdge4 =
105  Table[{-\[Pi] + 2 \[Pi] m/Nay, En[[m, indecesR[[2]]]], {m, 1, Nay}],
106
107 p1 = ListPlot[dispEdge1, Joined -> True];
108 p2 = ListPlot[dispEdge2, Joined -> True];
109 p3 = ListPlot[dispEdge3, Joined -> True];
110 p4 = ListPlot[dispEdge4, Joined -> True];
111
112
113 Show[{p1, p2, p3, p4}, PlotRange -> {{-\[Pi], \[Pi]}, {-3.2, 3.2}},
114 Frame -> True,
115 FrameLabel -> {"\!\(\(*SubscriptBox[\(k\), \(y\)]\)\)", "E"},
116 Axes -> False,
117 FrameTicks -> {Automatic,
118 None}, {{-\[Pi], -2 \[Pi]/3, -\[Pi]/3, 0, \[Pi]/3, 2 \[Pi]/3, \[Pi]}, None},
119 Joined -> True]
120
121
122
123 (*Offset*)
124 \[Delta] = 50;
125
126 Print["\nEdge states corresponding to IndecesR"]
127
128 (*Edge states for ky=\[Pi]/3, i.e. m=2Nay/3*)
129 Print["\nNo offset: ky=\[Pi]/3"]
130 ListPlot[Table[{m, vv[[2 Nay/3, indecesR[[2]], m]]}, {m, 1, Nax}],
131 Joined -> True, PlotRange -> All]
132 ListPlot[Table[{m, vv[[2 Nay/3, indecesR[[1]], m]]}, {m, 1, Nax}],
133 Joined -> True, PlotRange -> All]
134
135
136 Print["\nOffset \[Delta], R"]
137 ListPlot[
138  Table[{m, vv[[2 Nay/3 + \[Delta], indecesR[[2]], m]]}, {m, 1,
139  Nax}], Joined -> True, PlotRange -> All]
140 ListPlot[
141  Table[{m, vv[[2 Nay/3 + \[Delta], indecesR[[1]], m]]}, {m, 1,
142  Nax}], Joined -> True, PlotRange -> All]
143
144 Print["\nOffset -\[Delta], R"]
145 ListPlot[
146  Table[{m, vv[[2 Nay/3 - \[Delta], indecesR[[2]], m]]}, {m, 1,
147  Nax}], Joined -> True, PlotRange -> All]
148 ListPlot[
149  Table[{m, vv[[2 Nay/3 - \[Delta], indecesR[[1]], m]]}, {m, 1,
150  Nax}], Joined -> True, PlotRange -> All]
151

```

```

152 Print["\nOffset 2\[Delta], R"]
153 ListPlot[
154  Table[ {m, vv[[2 Nay/3 + 2 \[Delta], indecesR[[2]], m]}], {m, 1,
155   Nax}], Joined -> True, PlotRange -> All]
156 ListPlot[
157  Table[ {m, vv[[2 Nay/3 + 2 \[Delta], indecesR[[1]], m]}], {m, 1,
158   Nax}], Joined -> True, PlotRange -> All]
159
160 Print["\nOffset -2\[Delta], R"]
161 ListPlot[
162  Table[ {m, vv[[2 Nay/3 - 2 \[Delta], indecesR[[2]], m]}], {m, 1,
163   Nax}], Joined -> True, PlotRange -> All]
164 ListPlot[
165  Table[ {m, vv[[2 Nay/3 - 2 \[Delta], indecesR[[1]], m]}], {m, 1,
166   Nax}], Joined -> True, PlotRange -> All]
167
168
169 Print["\nEdge states corresponding to IndecesL"]
170
171 (*Edge states for ky=-2Pi/3, i.e. m=Nay/6*)
172 Print["\nNo offset: ky=-2Pi/3"]
173 ListPlot[ Table[ {m, vv[[Nay/6, indecesL[[2]], m]}], {m, 1, Nax}],
174 Joined -> True, PlotRange -> All]
175 ListPlot[ Table[ {m, vv[[Nay/6, indecesL[[1]], m]}], {m, 1, Nax}],
176 Joined -> True, PlotRange -> All]
177
178
179 Print["\nOffset \[Delta], R"]
180 ListPlot[
181  Table[ {m, vv[[Nay/6 + \[Delta], indecesL[[2]], m]}], {m, 1, Nax}],
182 Joined -> True, PlotRange -> All]
183 ListPlot[
184  Table[ {m, vv[[Nay/6 + \[Delta], indecesL[[1]], m]}], {m, 1, Nax}],
185 Joined -> True, PlotRange -> All]
186
187 Print["\nOffset -\[Delta], R"]
188 ListPlot[
189  Table[ {m, vv[[Nay/6 - \[Delta], indecesL[[2]], m]}], {m, 1, Nax}],
190 Joined -> True, PlotRange -> All]
191 ListPlot[
192  Table[ {m, vv[[Nay/6 - \[Delta], indecesL[[1]], m]}], {m, 1, Nax}],
193 Joined -> True, PlotRange -> All]
194
195 Print["\nOffset 2\[Delta], R"]
196 ListPlot[
197  Table[ {m, vv[[Nay/6 + 2 \[Delta], indecesL[[2]], m]}], {m, 1,
198   Nax}], Joined -> True, PlotRange -> All]
199 ListPlot[
200  Table[ {m, vv[[Nay/6 + 2 \[Delta], indecesL[[1]], m]}], {m, 1,
201   Nax}], Joined -> True, PlotRange -> All]
202
203 Print["\nOffset -2\[Delta], R"]
204 ListPlot[
205  Table[ {m, vv[[Nay/6 - 2 \[Delta], indecesL[[2]], m]}], {m, 1,
206   Nax}], Joined -> True, PlotRange -> All]
207 ListPlot[
208  Table[ {m, vv[[Nay/6 - 2 \[Delta], indecesL[[1]], m]}], {m, 1,
209   Nax}], Joined -> True, PlotRange -> All]
210
211
212
213 Print["\nDistribution R"]
214 ListPlot[Table[{-\[Pi] +
2 \[Pi] m/
Nay, (vv[[m, indecesR[[2]], 1]])^2 + (vv[[m, indecesR[[2]],
2]])^2 + (vv[[m, indecesR[[2]], Nax]])^2 + (vv[[m,
indecesR[[2]], Nax - 1]])^2}, {m, 1, Nay}], Joined -> True]
215 ListPlot[Table[{-\[Pi] +
2 \[Pi] m/
Nay, (vv[[m, indecesR[[1]], 1]])^2 + (vv[[m, indecesR[[1]],
2]])^2 + (vv[[m, indecesR[[1]], Nax]])^2 + (vv[[m,
indecesR[[1]], Nax - 1]])^2}, {m, 1, Nay}], Joined -> True]
216
217
218
219 Print["\nDistribution L"]
220 ListPlot[Table[{-\[Pi] +
2 \[Pi] m/
Nay, (vv[[m, indecesL[[2]], 1]])^2 + (vv[[m, indecesL[[2]],
2]])^2 + (vv[[m, indecesL[[2]], Nax]])^2 + (vv[[m,
indecesL[[2]], Nax - 1]])^2}, {m, 1, Nay}], Joined -> True]
221
222
223
224
225
226
227
228

```

```

229     2] ])^2 + (vv[[m, indecesL[[2]], Nax]]]^2 + (vv[[m,
230     indecesL[[2]], Nax - 1]]]^2}, {m, 1, Nay}], Joined -> True]
231 ListPlot[Table[{-\[Pi] +
232     2 \[Pi] m/
233     Nay, (vv[[m, indecesL[[1]], 1]]]^2 + (vv[[m, indecesL[[1]],
234     2]]]^2 + (vv[[m, indecesL[[1]], Nax]]]^2 + (vv[[m,
235     indecesL[[1]], Nax - 1]]]^2}, {m, 1, Nay}], Joined -> True]
236
237
238
239 End[]];

```

Listing 5: Mathematica script for HH Chern-Number numerical computation

```

1 Begin["Chern`"];
2 ClearAll["Chern`*"];
3
4 (*Berry curvature on a plaquette, with PBCs*)
5 (*z is a matrix ni*nj, with (i,j) element the eigenstate in the grid \
6 point (Subscript[k, x,i],Subscript[k, y,j]) *)
7 BerryCurvature[z_, i_, j_] := Module[{\[Gamma], ni, nj, CompDot},
8   CompDot[a_, b_] := Conjugate[a].b;
9   ni = Dimensions[z][[1]];
10  nj = Dimensions[z][[2]];
11  \[Gamma] = CompDot[z[[i, j]], z[[i, Mod[j + 1, nj, 1]]]];
12  \[Gamma] = \[Gamma]*CompDot[z[[i, Mod[j + 1, nj, 1]]],
13    z[[Mod[i + 1, ni, 1], Mod[j + 1, nj, 1]]]];
14  \[Gamma] = \[Gamma]*CompDot[z[[Mod[i + 1, ni, 1], Mod[j + 1, nj, 1]]],
15    z[[Mod[i + 1, ni, 1], j]]];
16  \[Gamma] = \[Gamma]*CompDot[z[[Mod[i + 1, ni, 1], j]], z[[i, j]]];
17  Arg[\[Gamma]]
18 ]
21
22 (*Sum over the plaquettes*)
23 TotalBerryCurvature[z_] := Module[{ni, nj},
24   ni = Dimensions[z][[1]];
25   nj = Dimensions[z][[2]];
26   Table[BerryCurvature[z, i, j](*/(2Pi)*), {i, 1, ni}, {j, 1, nj}]
27 ]
28 ChernNumber[
29   z_] := (1/(2 Pi)) Chop[
30   Sum[BerryCurvature[z, i, j], {i, 1, Dimensions[z][[1]]}, {j, 1,
31   Dimensions[z][[2]]}]];
32
33
34 ChernHamiltonian[\[Alpha]_, kx_, ky_] := Module[{a, t, Q, Hmatrix},
35   a = 1; (*Unit of length*)
36   t = 1; (*Unit of energy*)
37   Q = If[\[Alpha] > 0, Denominator[Rationalize[\[Alpha]]], 1];
38
39   Hmatrix = SparseArray[
40     {
41       {i_, j_} /; Abs[i - j] == 1 -> 1,
42       {i_, j_} /; Abs[i - j] == 0 -> 2 t Cos[ky a - 2 Pi \[Alpha] i],
43       {1, Q} -> t Exp[I kx Q a],
44       {Q, 1} -> t Exp[-I kx Q a]
45     }
46     , {Q, Q}, 0];
47   Hmatrix = Normal[Hmatrix];
48   Hmatrix
49 ]
50
51
52 test[\[Alpha]_, n_] := Module[{a, Q, Ncx, Ncy, Nax, Nay},
53   a = 1; (*Unit of length*)
54   Q = If[\[Alpha] > 0, Denominator[Rationalize[\[Alpha]]], 1];
55   Ncy = n;
56   Ncx = n;
57   Nax = Q n;
58   Nay = Ncy;
59   Table[Transpose[
60     Sort[Transpose[
61       Eigensystem[
62         N[ChernHamiltonian[\[Alpha], kx, ky]]]], #1[[1]] > #2[[
```

```

63      1]] &]][[2, 2]]
64 , {kx, 0, (2 Pi)/a*1/Nax (Ncx - 1), (2 Pi)/a*1/Nax}, {ky,
65 0, (2 Pi)/a*1/Nay (Nay - 1), (2 Pi)/a*1/Nay}]
66 ]
67
68
69 alpha = 1/3;
70
71 ListPlot[Table[{n, ChernNumber[test[alpha, n]]}, {n, 15, 20}]]

```

Listing 6: Mathematica script for Chern-Number determination by means of Diophantine solver

```

1 Begin["Diophanto`"];
2 ClearAll["Diophanto`*"];
3 Clear[P, Q, r, t];
4
5 P = 1;
6 Q = 3;
7
8 tlist = {0};
9 For[r = 1, r < Q + 1, r++,
10 tt = 0;
11 sol = FindInstance[P*t + Q*s == r && -Q/2 <= t <= Q/2, {t, s},
12 Integers];
13 tt = t /. sol[[1]];
14 tlist = Append[tlist, tt];
15 ]
16 Clist = {};
17 For[i = 2, i < Q + 2, i++,
18 Clist = Append[Clist, tlist[[i]] - tlist[[i - 1]]] ];
19 ]
20 Clist
21
22 (* ****)
23
24 Out[] = {1, -2, 1}

```